NTNU
Norwegian University of
Science and Technology

Study on initial stage of metal dusting corrosive on Inconel 601 and Incoloy 800

Jianyu Ma

Chemical Engineering and Biotechnology
Submission date: June 2017
Supervisor: Hilde Johnsen Venvik, IKP

Norwegian University of Science and Technology
Department of Chemical Engineering

Preface

This thesis is written as a completion of the MSc. program in Department of Chemical Engineering, Norwegian University of Science and Technology. The thesis was written during spring semester 2017, and it accounts for 30 credits.

Writing this report was a challenging but wonderful task, which not only provides me with theoretical knowledge, but helps me built well-rounded academic studying skills.

I would like to sincerely thank Professor Hilde J. Venvik, Xiaoyang Guo and Dr. Estelle Marie M. Vanhaecke for their excellent guidance and help.

I declare that this is an independent work according to the exam regulations of the Norwegian University of Science and Technology (NTNU).

Trondheim, December 14, 2016

Jianyu Ma

Abstract

Metal dusting is a corrosive phenomenon of metals or alloys into fine, dust-like particles. It can be found in many industrial units or processes, such as petrochemical industry.

Metal dusting is initiated by unwanted carbon formation on the inner surface of alloy equipment while the alloy is exposed to gas atmosphere with high carbon activity at high temperature and pressure. Carbon is formed by CO reduction or Boudouard reaction.

The main objective of this paper is to investigate how Fe-based (Incoloy 800) and Ni based (Inconel 601) alloy samples perform with different CO exposure time under high pressure metal dusting environment. All samples are polished and pretreated with steam oxidation. Then the samples are exposed to carburizing atmoshphere at 750 °C, at 20 bar in 100Nml/min gas flow with a $CO/H_2/CO_2/H_2O/Ar$ gas mixture of composition 20/25/15/10/30 (vol.%) for 10min to 20 h.

Samples after CO exposure are studied by scanning electron microscopy and Raman spectroscopy. And the results show that evident carbon formats on Inconel 601 surface, while no carbon formats on Incoloy 800 surface, however, composition change occurs.

Table of Content

List of figures

List of tables

Abbreviations

ΔH	Enthalpy change of a reaction
a_c	Carbon activity
k_1	Rate constant of metal wastage
k_2	Rate constant of carbon deposition
k_3	Rate constant of CH_4 decomposition
K_i	Equilibrium constant of a reaction
T	Reaction temperature

Chapter 1. Introduction

1.1 Introduction into metal dusting

Metal dusting is a catastrophic form of corrosion that attacks Fe-based and Ni-based alloys exposed to carburizing environments at high temperature. Carbon arises on the alloy surface and dust-like metal powder is produced while disintegrating the metal or alloy structure [1]. This is a critical issue in the industry of petrochemicals, specifically in reforming units and cracker furnaces, where alloy units suffer gas atmosphere with high carbon activity (**Figure 1. 1**). It is also possible arising in high-temperature fuel cells, such as solid oxide fuel cell and molten carbonate fuel cell [2].
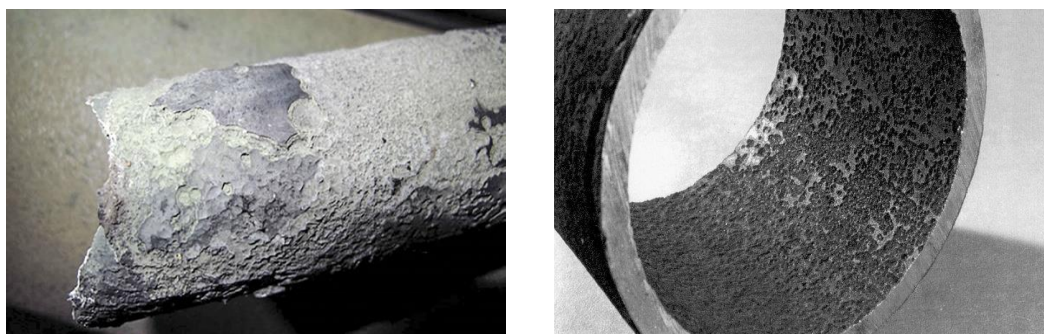
Figure 1. 1 Metal dusting corrosion form industrial plants

Metal dusting attacks the alloy surface and leave pits and holes on high alloy steels （with high content of Cr, Al and other metal elements), or metal wastage on low alloy steels (with low content of Cr, Al), respectively [3]. Carbon powder growing on the metal surface is easily carried away with gas flux at high velocity in industrial units, which might foul the downstream process or equipment.

Controlling and reducing metal dusting corrosion needs to be taken into consideration since it poses issues to production units. The main method to eliminate the influence of metal dusting on equipment currently is replacing the corroded section, and detailed monitoring and periodic inspection are required as well. While these add large extra costs. For example, the US Department of Energy has reported that annually 220-290

million dollars is spent to replace unit due to metal dusting corrosion in hydrogen production industry [4].

1.2 Scope of the present work

Since metal dusting corrosion was first described in 1945 by E. Camp and his colleagues [1], it became a well-known issue in the chemical industry and widely studied. A number of literatures reported the process of metal dusting in the alloy matrix once carbide phases formed, as well as the potential chemical and physical protection methods. But the kinetics of initial stage of metal dusting, especially under high pressure environment, was less described.

Metal dusting corrosion starts from undesired carbon formation on the metal surface, especially on alloy containing Fe, Ni or Co. It is kinetically controlled, which means it is influenced by temperature, partial pressure, nanostructure and composition of alloy surface. Under the synthesis gas environment, CO reduction, Boudouard reaction and alkane cracking reactions are the main sources of carbon formation. The reactions are strongly affected by reaction conditions, such as temperature and partial pressure of CO. Nanostructure of surface, containing the grain boundary size, poses impact on corrosion degree as well. While Cr and Al can be added in to alloy and play a role of corrosion protection though forming an oxide layer to isolate the underlying alloy bulk to the carburizing atmosphere. Hence, developing better protection oxide layer can be an effective method to mitigate metal dusting corrosion.

The main objective of this paper is to investigate how alloy samples perform on the initial stage of metal dusting. CO exposure experiments with different time scale were carried out to study nanostructure and composition changes on alloy surface along CO exposure time. And two series of alloys will be applied, Ni-based alloy (Inconel 601) and Fe-based alloy (Incoloy 800), comparison of anti-corrosion resistance between these two alloys will be conducted as well.

Chapter 2. Theory and Literature review

2.1 Reactions and carbon activity

Metal dusting is a corrosion phenomenon where undesired carbon forms on the inner surface of alloy equipment under a carburizing gas atmosphere at high temperature (400~800 °C), normally encountered in the plants for petrochemical products, natural gas processing, coal gasification, etc. The corrosion reveals itself as breaking up the bulk metal into metal powder. Carbon formation potential on alloy under the carburizing atmosphere is the key to understand the whole process thermodynamics. Meanwhile, the process is also strongly controlled by kinetics, including the catalysis and the reaction condition. Plenty of efforts have been paid to build a systematical theory about the thermodynamic and kinetic description, which can be applied to understand, predict and prevent metal dusting corrosion. In this chapter, a brief theoretical introduction to thermodynamics and kinetics of metal dusting will be given.

2.1.1 Thermodynamics

The precursor for metal dusting is unwanted carbon formation on the alloy surface of process equipment, which are subjected to gas mixture containing synthesis gas (CO and H_2), steam, CO_2 or CH_4, mostly at temperature range from 400 to 800°C. The main reactions contributing to carbon formation are the Boudoard reaction and CO reduction [1,2,6,7].

- The Boudoard reaction:

$$2CO = C + CO_2 \qquad\qquad \Delta H_1 = -172.4 \text{ kJ/mol} \qquad\qquad (2.1)$$

- The CO reduction reaction:

$$CO + H_2 = C + H_2O \qquad\qquad \Delta H_2 = -131.3 \text{ kJ/mol} \qquad\qquad (2.2)$$

The two reactions are both highly exothermic, which means they are thermodynamically favored by lower temperature. Considering about kinetics, however, higher temperature provides faster reaction rate. Hence, an optimized temperature window of approximately 400~800 °C was defined.

Water-gas shift reaction can also take place in case of the presence of steam in gas mixture, i.e. gas mixture in steam reforming process. WGS reaction contributes to changing gas atmosphere composition instead of carbon formation on alloy surface, which makes it hard to decide which carbon forming reaction is dominating.

● Water -gas shift reaction:

$$CO + H_2O = CO_2 + H_2 \qquad\qquad \Delta H_3 = \text{-41.2 kJ/mol} \qquad (2.3)$$

Sometimes hydrocarbons are present in the gas mixture, therefore, alkane cracking reactions is another source of undesired carbon formation, e.g. methane decomposition reaction

● CH$_4$ decomposition

$$CH_4 = C + 2H_2 \qquad\qquad \Delta H_4 = \text{75.6 kJ/mol} \qquad (2.4)$$

While the difference is that alkane cracking reactions are exothermic, which are favored at high temperature. Therefore, alkane decomposition might domain carbon formation at relatively high temperature.

To describe the driving force of carbon formation, the thermodynamic parameter, carbon activity (a_c), is commonly utilized [1,6,7]. Higher carbon activity of gas composition means larger potential of carbon formation on the metal surface exposed to metal dusting atmosphere. Carbon activities of the reactions mentioned above can be calculated as followed:

● CO reduction reaction

$$a_c = K_1(T)\left[\frac{P_{CO}P_{H_2}}{P_{H_2O}}\right] \qquad (2.5)$$

● Boudouard reaction

$$a_c = K_2(T) \left[\frac{P_{CO}^2}{P_{CO_2}} \right] \qquad (2.6)$$

- CH$_4$ decomposition

$$a_c = K_3(T) \left[\frac{P_{CH_4}}{P_{H_2}^2} \right] \qquad (2.7)$$

Where $K_i(T)$ is the equilibrium constant of the reaction and P_i represents the partial pressure of the corresponding gas component. And from the equations we can see, carbon activity is function of temperature and partial pressure of gas components. By definition, metal dusting only starts when the gas phase carbon activity is greater than the unity ($a_c \gg 1$) [6].

Reaction 2.1, 2.2 and 2.3 are three main sources of undesired carbon formation, normally one or more of these three reactions may be involved. Besides of the reactions above, carbide decomposition also produces solid carbon on iron-based alloy surface [1,7]

$$Fe_3C_{(s)} = C_{(s)} + 3Fe_{(s)} \qquad (2.8)$$

This reaction normally occurs under atmosphere with relatively low carbon activities ($a_c \leq 1$) due to thermodynamic instability of Fe$_3$C. Other carbon formation reactions involving metal element were reported as well[1,2]. For example

$$CO_{(g)} + M_{(s)} = C_{(s)} + MO_{(s)} \qquad (2.9)$$

$$CO_{2(g)} + 2M_{(s)} = C_{(s)} + 2MO_{(s)} \qquad (2.10)$$

Here, M means a metal particle generated during metal dusting process, MO means metal oxide.

2.2 Mechanism of metal dusting

As mentioned above, metal dusting begins with the carbon formation on the surface of metals or alloy under carburizing environment, and one or several of three reactions (reaction 2.1,2.2 and 2.4) might be the initial carbon source. However, the formation of surface carbon is also strongly controlled by kinetics. Carbon formation reactions

mentioned above (2.1, 2.2 and 2.4) are catalyzed by certain metals. Ni, Fe and Co, as well as their alloys, are all susceptible to metal dusting, in the meanwhile, among the mostly used components of high temperature alloys. Thus, kinetic is influenced by catalytic properties such as alloy composition and nanostructure [1,2,3]. Besides of that, it is also influenced by the local condition such as temperature and partial pressure of carbon containing gas component.

Possible mechanistic steps of carbon transfer from gas phase to alloy surface via reaction 2.1, 2.2 and 2.3 are listed in **Table 2. 1**. Reactions written in bold letters and underlined are the rate determining steps (RDS) for each of three potential carbon formation reactions, respectively [7,8,9]. Absorbed CO molecule dissociation is RDS for CO reduction reaction; absorbed CO_2 formation and desorption are RDS for Boudouard reaction.

Adsorbed carbon *(C*)* dissolved onto alloy surface and reacts with metal elements, such as Fe, into carbide [1]. For Fe-containing alloy, iron carbide can be formed under high carbon activity condition,

$$3Fe + C_{(dissolved)} = Fe_3C \qquad\qquad (2.11)$$

The dissolved carbon can also combine with other metal elements and form carbides [1]

$$M + C_{(dissolved)} = MC \qquad\qquad (2.12)$$
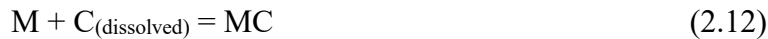
Where M = Cu, Ti, W, V

Or when M is Cr,

$$M + C_{(dissovlved)} = M_7C_3 \text{ and/or } M_{23}C_6 \qquad\qquad (2.13)$$

As an important element widely applied in alloy, Ni forms carbide under carburizing environment. However, Ni carbide is not stable that metal dusting on Ni or Ni-based alloy going through different pathway, which will be described in detail later.

Table 2. 1 Mechanistic steps for carbon formation via CO reduction, Boudouard and CH$_4$ decomposition reactions, where * means vacant active site [1].

CO reduction reaction	Boudouard reaction	CH$_4$ decomposition reaction
CO (g) + * ↔ CO*	CO (g) + * ↔ CO*	CH$_4$ (g) + * ↔ CH$_4$*
CO* + * ↔ C* + O*	CO* + * ↔ C* + O*	CH$_4$* + * ↔ CH$_3$* + H*
H$_2$ (g) + 2* ↔ 2H*	**CO* + O* ↔ CO$_2$* + ***	**CH$_3$* + * ↔ CH$_2$* + H***
H$_2$ (g) + O* ↔ H$_2$O (g) + *	**CO$_2$* ↔ CO$_2$ (g) + ***	CH$_2$* + * ↔ CH* + H*
H$_2$O (g) + * ↔ H$_2$O*	**CO (g) + O* ↔ CO$_2$ (g) + ***	CH* + * ↔ C* + H*
H$_2$O* + * ↔ OH* + H*	nC* ↔ nC (s) + n*	nC* ↔ nC (s) + n*
OH* + * ↔ O* + H*	C* ↔ C (dissolved) + *	C* ↔ C (dissolved) + *
2OH* ↔ H$_2$O* + O*		
nC* ↔ nC (s) + n*		
C* ↔ C (dissolved) + *		

Despite the mechanism of metal dusting has been investigated intensively, there is no generally accepted theory yet. The most widely accepted metal dusting mechanism for Fe, Ni or their alloy materials is proposed by *Grabke et al* [7,8]. The mechanism for Fe or Fe-based steel includes the following steps:

- Carbon is transferred from gas phase into the solid phase through reactions (2.1), (2.2) and (2.4) mentioned above under the environment with high carbon activity.

- Fe in the alloy reacts with the carbon and forms iron carbides, i.e. Fe$_3$C (cementite). The reaction takes place mainly at the surface or, to some degree, on the grain boundaries. The carbide layer plays a role as barrier for further carbon intrusion because of its low carbon diffusivity.

- Newly formed carbide section leads to beginning of graphite growing outward to the surface.

- The carbide forming at interface of graphite-carbide is unstable, as a result carbon activity at the interface is lower than that in the iron carbide. Fe_3C therefore begins to decompose into C and Fe.

- The freshly released fine Fe particles are a super excellent catalyst that it catalyzes the formation of solid carbon when it diffuses to the gas-graphite interface. And it also boosts process repeats from the first step with much high reaction rate.

Mechanism for metal dusting on Ni is similar as it on Fe, the only difference is that nickel carbide is too unstable to form. The process thus involves direct carbon growth into the Ni or Ni containing alloy. Detailed steps are described later.

2.3 Metal dusting corrosion of different materials

2.3.1 Metal dusting corrosion of iron and low-alloy steels

Metal dusting corrosion of Fe and Fe-based materials with low Cr content (low-alloy steels are found to follow the mechanism mentioned before at the temperature lower than 700°C, including steps of carbon formation, carbon diffusion, carbide formation, graphite formation and subsequent carbide decomposition. At temperature higher than 700 °C, Fe and low-alloy steel follow the same degradation mechanism, with a thin Fe layer forming at graphite-carbide interface instead of generation of Fe particles. At further higher temperature(>900°C), carbon formation reaction, such CO reduction and Boudouard reaction, are quite slow due to low thermodynamic driving force, hence, metal dusting process is slow, either [7,8].

2.3.2 Metal dusting corrosion of high-alloy steels

High-alloy steels, comprising high amount of Cr and other elements like Ti, V, W, can form specific oxide layer acting protection function, for example, Cr-oxide layer.

However, carbon formation may start from certain points with defect of oxide layer, and it leads to pitting and holes formation on the alloy surface. **Figure 2. 1** illustrates the process of metal dusting on high-alloy steels. Firstly, carbon transfer from gas phase to alloy matrix where there are defects on the oxide layer. The dissolved carbon and metal elements, such as Cr, Ti, combine as stable carbides, and with the quantity of carbides increasing, carburization oversaturates the carbide region and forms metastable carbides at gas solid interface. Then graphite forms and the further growth of graphite lowers the local carbon activity and destabilizes the unstable carbides. The carbide decomposes to graphite, which grows into the alloy, and metal particles diffuse though the graphite to gas-graphite interface, catalyzing carbon deposition further [1,9].
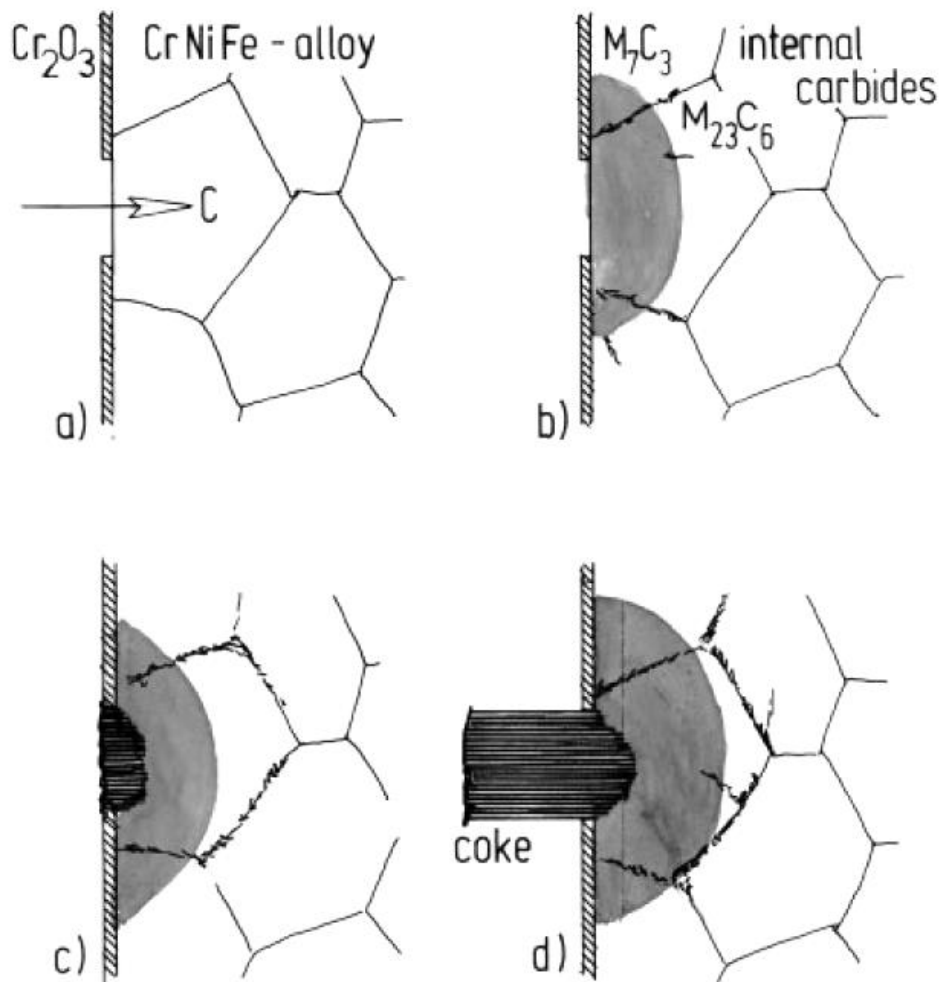
Figure 2. 1 Schematic illustration of metal dusting corrosion of high alloy steels, proposed by *Grabke et al.* [9]

2.3.3 Metal dusting corrosion on Ni or Ni-based steels

As mentioned above, the Ni carbides are too unstable to be identified at metal dusting condition, hence, metal dusting on Ni and Ni-based alloys emerges directly by graphite carbon penetrating into the material. It follows steps below [9]:

■ Carbon transfer from gas phase to solid phase;

■ Carbon/graphite forms on the surface (carburize surface);

■ Carbon is oversaturated at surface area with carbon in solid solution. And graphite grows into the alloy matrix with addition of carbon in solid solution;

■ Graphite carbon grows inward and destructs alloy matrix, as a result, metal particles drop off from matrix to the gas-graphite interface

■ Fine metal particles play a role as catalysts for further graphite formation.

Zeng and co-workers [10] proposed a mechanism based on carbon crystallization transferring. The firstly deposited carbon on surface is poorly crystalized, while they will diffuse into the Ni or Ni-based alloy matrix. The carbon diffusing inward forms more crystalized carbon and grows outward, leading to breaks of alloy. It might obey the following steps:

■ Carbon transfers from gas phase to alloy surface

■ Poorly crystallized carbon dissolve in nickel because it shows slightly higher saturating concentration than that of graphite and the saturating concentration of poorly crystallized carbon will be oversaturating for graphite. The dissolved carbon accumulates at defects as well crystalized carbon;

■ Free energy gap between poorly crystallized carbon and well-crystallized graphite drives carbon to diffuse inward and precipitate, leading to expansion of growth of carbon phase inside alloy matrix. The accumulation of causes breaks-up of alloy (**Figure 2. 2**) and some metal particles are separated from alloy matrix;

■ Carbon phase continuously grow and Ni particles falling off from the materials can catalyze the formation of carbon filaments (**Figure 2. 3**).
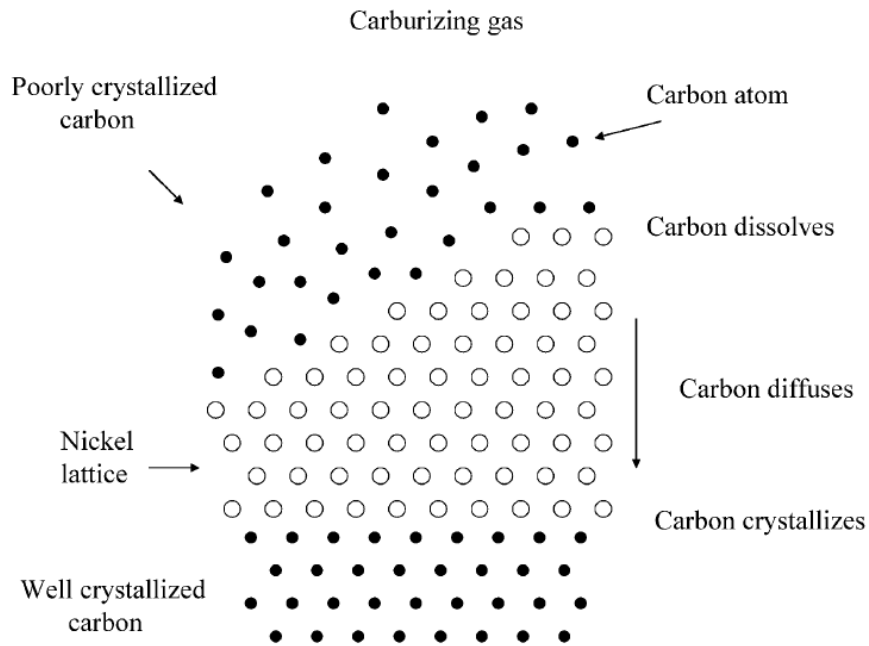
Figure 2. 2 Disoriented carbon dissolves in and diffuses through nickel; the lattice plane of nickel gives excellent orientation to improve crystallinity of carbon [10].
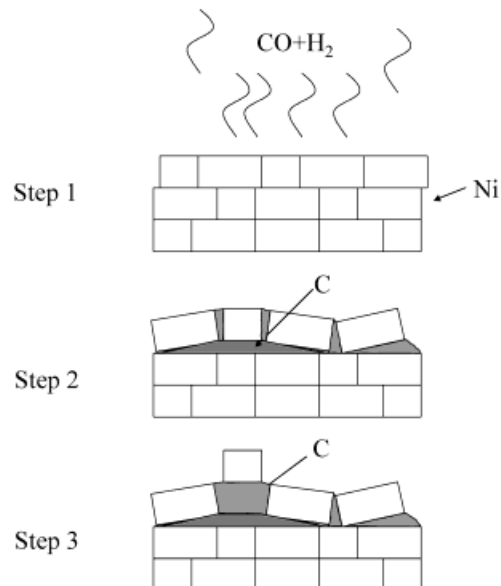
Figure 2. 3 Carbon particles precipitate at the defects in nickel. Accumulation of carbon particles causes nickel to separate into small particles and the resultant small particles move away from the metal [10].

2.4 Prevention techniques and the limitations

To minimize impact of metal dusting on alloy furnace component, several methods have been suggested. They can be roughly divided into the categories listed below [10]:

(1) **Adjusting process conditions**. As mentioned before, metal dusting (without CH_4) only occurs when carbon activity $a_c > 1$ and the system temperature range between 400~800°C. Reducing carbon activity of gas atmosphere or adjusting process temperature out of the range 400~800°C is a possible solution to mitigate the harmful corrosion. While this temperature range is the optimized temperature condition carried out in most of practical industrial processes considering about the thermodynamic factor. On the other hand, adjusting process condition might avoid metal dusting, however, it leads to low producing efficiency and economical benefit. For example, adding additional steam or air to lower the carbon activity will increase the operation cost. Therefore, it is not an ideal option to change the conditions due to the strict process requirement.

(2) **Surface poisoning**. Metal dusting could be resisted by adding proper poisoning element into gas flue, which is adsorbed onto the metal surface more firmly than carbon and eliminate carbon formation. Sulphur is typical poisoning agent. For example, sulfur carrying compounds can be added into gas atmosphere, such as dimethyl disulfide which decomposes into H_2S [11]. H_2S and the metal surface build-up thin sulfide layer through the reaction: $H_2S = H_2 + S_{ads.}$ The layer retards decomposition of carbon carrying gas compounds and suppress metal dusting. While adjusting strictly required amount of H_2S is crucial, since overfeeding bring excessed sulfidation and poison the catalysts downstream, underfeeding leads to insufficient prevention. And a sulphur removal unit should be installed to avoid damage to processing equipment. Phosphorous is another option as poisoning compound to avoid metal dusting, while it reveals similar issues as Sulphur [12].

(3) **Formation of surface oxide layer**. The alloy element, such as Cr, Al [11,13], can form oxide layers with pretreatment, which separate the base material from the corrosive atmosphere. Large amount of Cr with less amount of Al, Si and Mn are often mixed into alloy to form prevention oxide layer and shows great performance. I. Wolf and colleagues illustrated that the solubility of carbon in Cr_2O_3 or Al_2O_3 at 1000°C is below the detectability limit of ppm for radioactive ^{14}C. Moreover, the amorphous or metastable alumina phases grows slowly into dense oxide layer and are stable at the gas atmosphere with low oxygen partial pressure. The prevention function relies on the stability of oxide layer under special environment, such extremely high temperature or reducing condition. The properties of oxide, including its composition, thickness, density, uniformity and self-healing capability, determine its performance under carburizing atmosphere [14]. Hence, forming a uniform and stable oxide layer is challenge.

(4) **Coating**. Coating is relatively novel approach to suppress metal dusting corrosion by insulating alloy surface and carburizing gases with a thin, stable and protective layer [12]. The layer is usually produced by metal materials which has strong catalytic inhibition to carbon and good adherence to alloy substrate, such as Cr or Al oxide.

Coating materials and coating production methodology have been intensively researched recently. *C. Rosado* and *M. Schűtze* [11] proposed that the resistance of a material to metal dusting depends on the ability of the material to develop a protective oxide scale. Al, Si and Cr have been chosen to produce coatings on account of their ability to form stable protective oxide layer. They also have specific features in coating matrix, repectively

➤ Al. Formation of protective oxide layer (Al_2O_3 or with chromium (Al, Cr)-oxide) which are thermodynamically very stable.

➤ Si. Formation of protective oxide (SiO_2) which is thermodynamically very stable. Si can promote coating ductility.

➢ Cr Acts as inter-diffusion barrier for Al and forms oxide.

J. Alvarez and his colleague [17] studied Cr and Cr + oxide deposition coating on protecting materials subjected to metal dusting corrosion. They showed very strong metal dusting resistance, and the microstructure and the flexibility of the deposition method were promising as well.

Applying coating to avoid metal dusting possesses several advantages [11]:

1) Modification of processing conditions is not required;

2) Can be applied on existing alloys with good mechanical properties

3) Can be repaired/reapplied easily

While it also presents some limitations, such as

1) While the lifetime of coating is often limited by adhesion issue. Decreasing of adhesion between coating and substrate will lower the stability of coating nanostructure, creating a pathway for carburizing gas to diffuse into coating and access to the surface of substrate.

2) Relatively low thermal and hydrothermal stabilities could also lead to loss of function.

3) Long-term coating thermal expansion coefficient, which may have large impact on coating adhesion, is doubtable.

4) Additional coating layer means additional investment, which limits the application of coating to a large extent. Other factors, such as thermal conductivity, should be considered as well.

2.5 Summary

Metal dusting is a corrosion phenomenon in which metal or alloy surface exposed to carbon supersaturated gas atmosphere breaks into fine particles. It usually occurs between 400 °C to 800 °C, and several reactions contribute to carbon formation on the

alloy surface, mainly CO reduction and Boudoard reaction. Carbon formation is thermodynamically favored at low temperature, while further carbon extension and metal dusting progress are controlled mostly by kinetics. Fe and Ni play catalytic roles within the metal dusting process, and other factors, such as surface microstructure, influence as well. Different mechanisms of metal dusting on different materials' surfaces are proposed in the literatures. Different preventive methods also exist to minimize the reverse impacts of metal dusting, consisting of physical method (adjusting operation condition, laser treatment), chemical method (pre-oxidation, surface poisoning) and coating application. However, there are also disadvantages, e.g. costs, existing as well.

A large number of efforts have been paid into metal dusting study and a systematic understanding of its progress in the solid matrix is established. However, issues involved on the initial stage are less evident. For example, why some area is more sensitive to carbon deposition? How deposited carbon diffuse through metal oxide layer? Consequently, a series CO exposure experiments with different time scale under sever metal dusting environment are carried out in the paper. By applying more intensive carburizing condition, metal dusting process on tested samples will be accelerated. In the meanwhile, experiments with different time scales leads to the results terminate at different stages of metal dusting process. Thereby exact scenes, such as first carbon deposition from gas phase to solid phase, beginning of carbon filament formation, might be found on different samples. Then the whole initial stage of metal dusting process could be well studied and described with help of advanced characterization methods.

Chapter 3. Materials and Methods

3.1 Materials and preparation

Two different industrially applied alloy materials have been investigated in this work.

- Ni-based alloy Inconel 601
- Fe-based alloy Incoloy 800

Inconel 601 was a widely-used alloy mostly containing nickel, chromium and iron with a little quantity of several other elements (e.g. Al, Mn, Si, C). It has excellent resistance to corrosion under high temperature and shows good mechanical properties. Typical Inconel 601 composition matrix is listed in **Table 3. 1**.

Table 3. 1 Properties of Inconel 601[18]

Limiting Chemical Composition (%)	Ni......58.0-63.0 Cr......21.0-25.0 Al......1.0-1.7		Fe......Remainder C......0.10 max Mn......1.0 max	Si......0.50 max S......0.015 max Cu......1.0 max
Physical constants and thermal properties	Density	g/cm^3		8.11
	Melting Range	°C		1360-1411
	Specific Heat	J/kg•°C		448
	Coefficient of Expansion	20-100°C, μm/m•°C		13.75
	Thermal Conductivity	W/m•°C		11.2
	Electrical Resistivity	μΩ•m		1.19

The bulk composition of Inconel 601 coupon applied in the experiment is confirmed by Daham Gunawardana through EPMA/WDS[1]. The result, shown in **Table 3. 2**, fulfills the limited composition of Inconel 601.

Table 3. 2 Bulk composition of Inconel 601 alloy, determined by EPMA/WDS [1]

Composition Basis	Element percentage								
	Ni	Cr	Fe	Al	Mn	Ti	Si	Cu	C
atomic	57.65	24.31	13.33	2.64	0.60	0.36	0.15	0.17	0.77
weight	60.82	22.71	13.38	1.28	0.60	0.31	0.08	0.19	0.17

Alloy Incoloy 800 is a Fe-based alloy with good strength and excellent resistance to oxidation and carburization in high-temperature atmosphere. And comparing to Inconel 601, Incoloy 800 has significantly lower cost due to its higher Fe content. Typical Incoloy 800 composition matrix is listed in **Table 3. 3**.

Table 3. 3 Properties of Incoloy 800[18]

Limiting Chemical Composition (%)	Ni......30.0-35.0 Cr......19.0-23.0 Al......0.15-0.60 Ti......0.15-0.60		Fe......39.5 min C.......0.10 max Mn......1.5 max	Si......1.0 max S......0.015 max Cu......0.75 max
Physical constants and thermal properties	Density	g/cm^3		7.94
	Melting Range	°C		1357-1385
	Specific Heat	J/kg•°C		460
	Coefficient of Expansion	20-100°C, μm/m•°C		14.4
	Thermal Conductivity	W/m•°C		11.5
	Electrical Resistivity	μΩ•m		0.989

The bulk composition of Incoloy 800 coupon we applied in the experiment is obtained by Xiaoyang Guo[5] via EPMA/WDS. The result, shown in **Table 3. 4**, is found to be in agreement with the specification of the industrial alloy.

Table 3. 4 Bulk composition of Incoloy 800 alloy, determined by EPMA/WDS [5]

Composition basis	Element percentage (%)								
	Fe	Ni	Cr	Mn	Al	Si	Ti	Cu	C
Avg. atomic	45.92	28.40	22.57	1.08	0.71	0.65	0.26	0.13	0.25
Avg. weight	47.53	30.56	21.06	1.10	0.32	0.34	0.23	0.21	0.06

3.2 Sample preparation

Samples of Inconel 601 and Incoloy 800 industrial alloys were obtained by cutting 15×8 mm^2 coupons from a 0.5 mm thick sheet. A sub-set of coupons were subjected to the grinding and polishing subsequently.

The alloy samples attached to a metal mold with water, which helped to fix the sample during grinding and subsequent polishing. The sample was subjected to grinding with P800 (20 μm), P1200 (P2500 (10 μm) grit SiC papers, then subjected to polishing with 6 μm, 3 μm and finally 1 μm diamond dusts to give a mirror appearance. At the end of each grinding and polishing step the samples were cleaned with water and ethanol in a row.

All the samples (both Inconel 601 and Incoloy alloy) were ultrasonically cleaned in hexane (99%) and then dried overnight before the experiments.

3.2 Setup setting

All alloy samples were subjected to different gas atmospheres. Polished Inconel 601 and Incoloy 800 samples were subjected to oxidation pre-treatment and carbon monoxide (CO) exposure treatments under controlled conditions.

Figure 3. 1 shows a simplified flow scheme of the reactor setup used for experiments. Detailed flow scheme is shown in Appendix 2. Two alloy samples, Inconel 601 and Incoloy 800 respectively, were hung inside a vertical reactor tube enclosed in a furnace. The tube reactor is made from Incoloy 800H, inner surface of which was covered with gold to minimize the metal dusting corrosion [1] (**Figure 3. 2**). Two alloy samples tests were conducted simultaneously and hung inside the reactor with quartz rod.
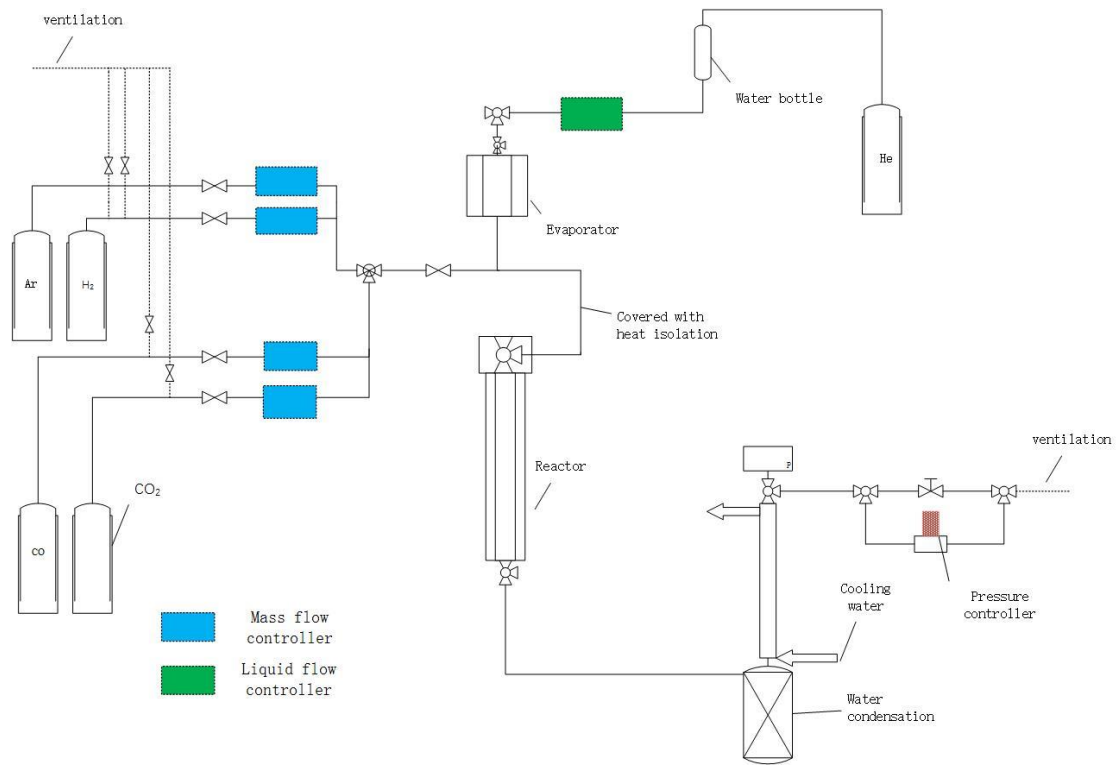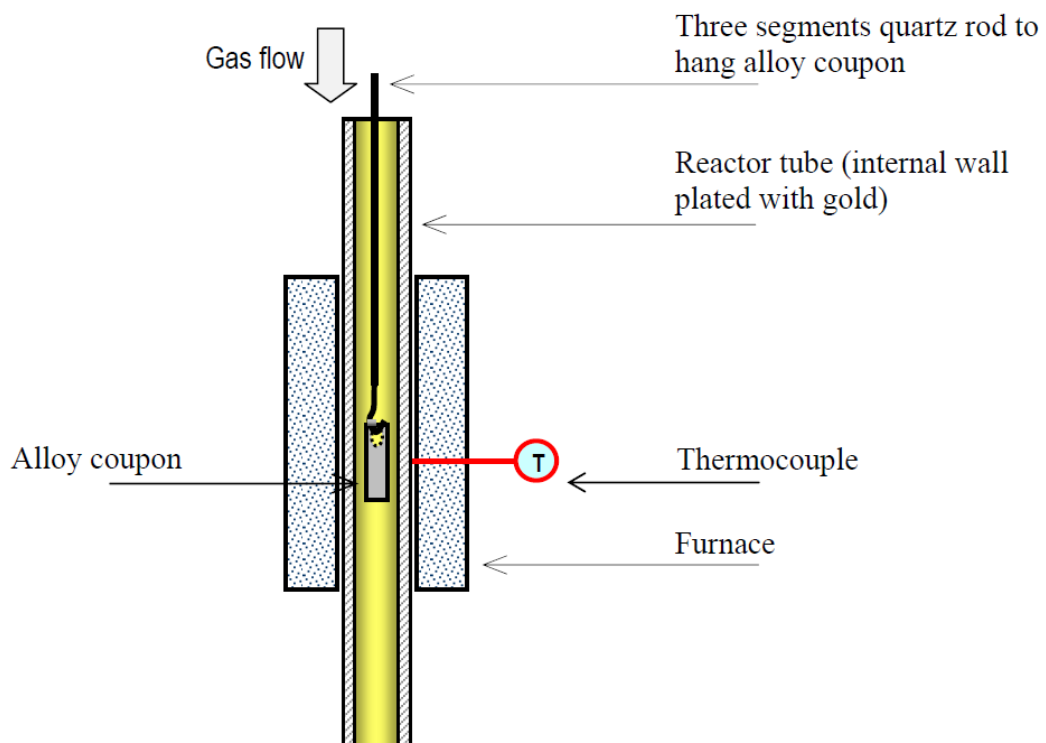
Figure 3. 1 Simplified schematic diagram of setup

Figure 3. 2 Schematic of sample mounting inside the reactor [1].

3.3 Exposure test

Required gas compositions flow rate were controlled by Bronkhorst HI-TEK mass flow controllers, and required steam flow rate was achieved through limit water flow with Bronkhorst HI-TEK liquid flow meter. The required amount of water flow directly into an evaporator and was heated into the steam under super high temperature. System pressure was measured and controlled by using Bronkhost EL-PRESS electronic pressure controller. All the controllers were regulated by Bronkhost controller-readout boxes. Temperatures of heating zones were monitored using type-K thermocouples and the furnace temperature was controlled by a Eurotherm 2416 controller [1].

3.3.1 Oxidation treatment

Oxidation treatment was implemented while keeping pressure at 1 bar and temperature at 540°C. The oxidation condition is selected from previous work in our group [1,5], relative metal oxides form within the step. Total gas flow rate was 100 Nml/min, and the composition of the gas mixture was 10% steam/90% Ar. Temperature ramping rate was 10°C/min. The sample was dwelled for 6h, with some samples analyzed as oxide and the others subjected to CO exposure subsequently.

3.3.2 CO exposure treatment

After the oxidation treatment, the reactor was ramped up to 750°C, with ramping rate 10°C/min, in the meanwhile, the pressure was increased to 20bar with maximum Ar flow. When it reached the desired temperature(750°C) and pressure(20bar), whole system retained the state for 20min to eliminate heating delay and stabilize the temperature inside. After 20min stabilization, CO containing gas mixture was introduced into the system. Total flow rate is 100 Nml/min and the composition is 20%CO, 25%H_2, 15%CO_2, 10%COsteam, 30%Ar. CO exposure was carried out with a range of dwelling time: 10min, 30min, 1h, 5h, 10h and 20h. **Figure 3. 3** shows the

temperature control profile of exposure treatments and the test matrix is listed in **Table 3. 5**. The results will be discussed later in Chapter 4.
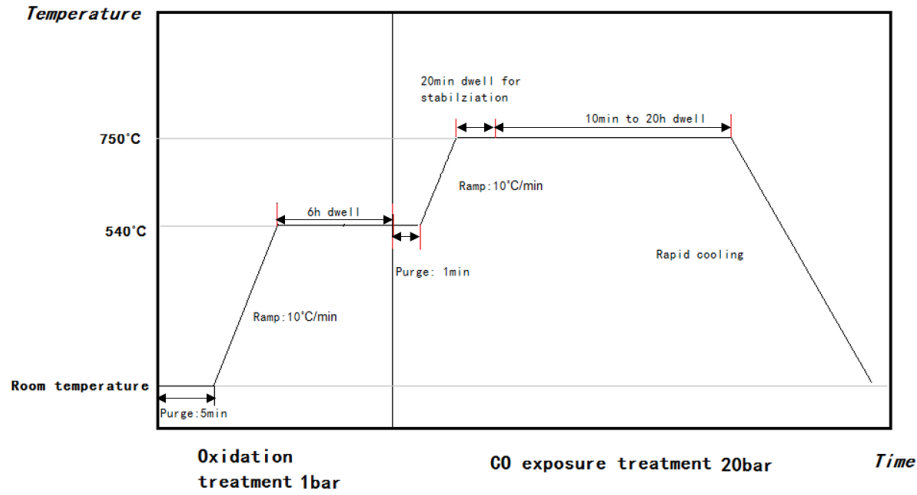
Figure 3. 3 Temperature profile of experiments

Table 3. 5 Exposure test matrix

Experiment No.	Oxidation	Carbonizing		Sample Code
		Condition	Time	
1			10min	601
2				800
3			30min	601
4				800
5	10% steam/ 90% Ar, 100ml/min flow rate, 540 °C, 1 bar, 6h	20%CO, 25%H$_2$, 15%CO$_2$, 10%COsteam, 30%Ar, 750°C, 20bar	1h	601
6				800
7			5h	601
8				800
9			10h	601
10				800
11			20h	601
12				800

3.4 Characterization techniques

3.4.1 Scanning electron microscopy (SEM)

Reacted samples with carburizing gas were investigated by field emission scanning electron microscope, Zeiss, SUPRA 55 FE-SEM. SUPRA 55 FE-SEM is a general

purpose ultra-high resolution SEM, providing morphological, topographical and compositional information as well as crystal orientation and structure or electronic defects. **Figure 3. 4** shows the simplified mechanism scheme of SEM, and **Figure 3. 5** shows the appearance of the SEM used in this project.

Figure 3. 4 Schematic representation of the essential components of SEM [20]
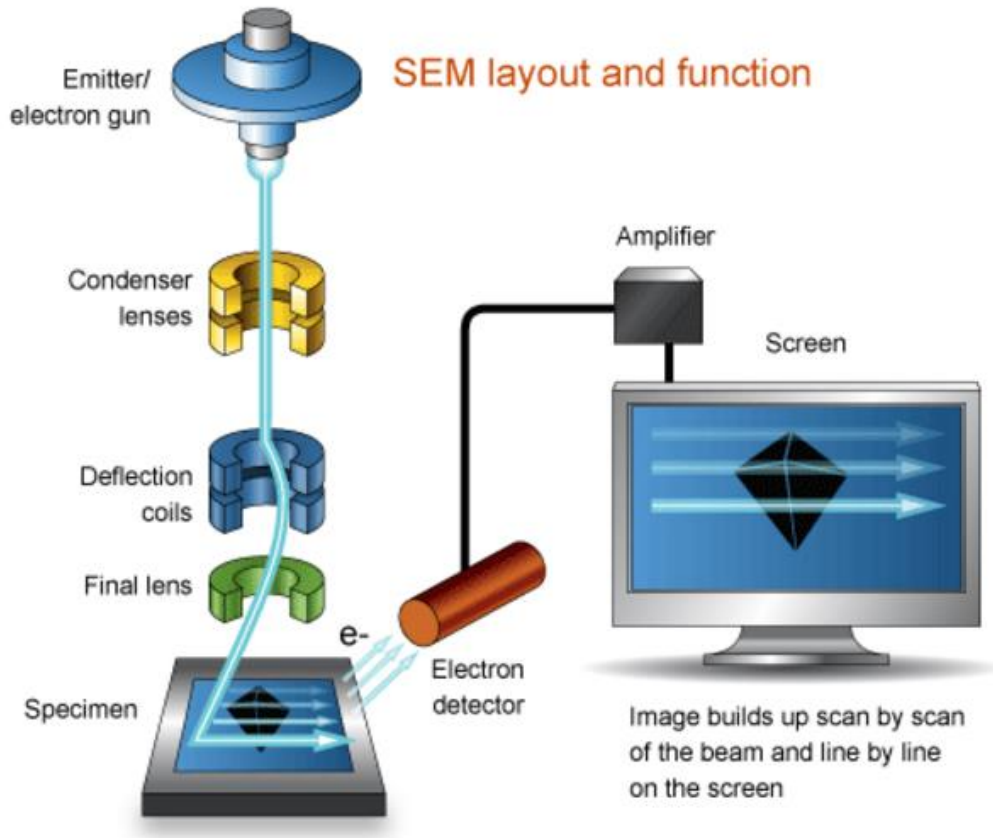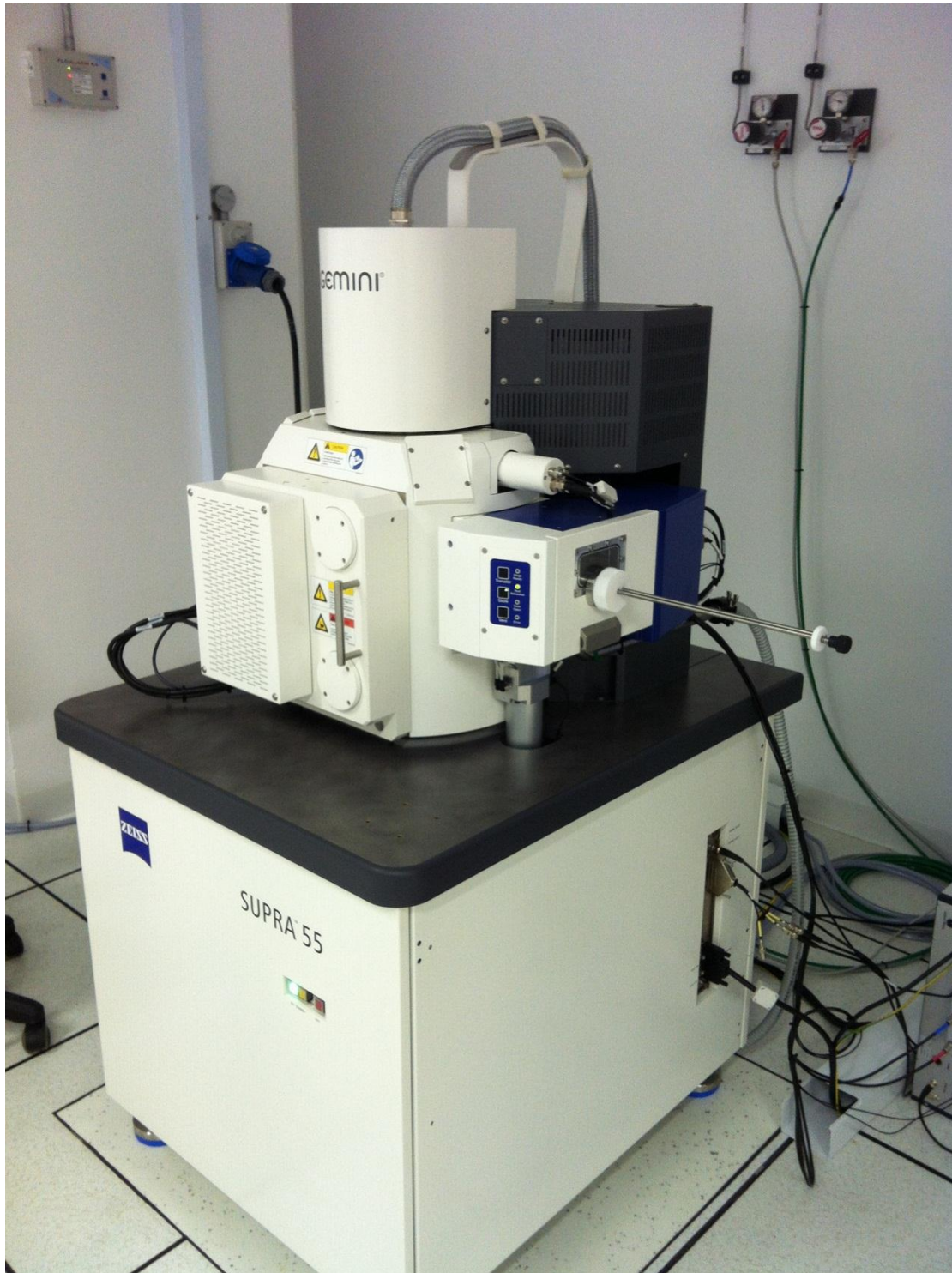
Figure 3. 5 Picture of ZEISS, SUPRA 55

The SEM uses a beam of high energy electrons generated by an electron gun, processed by magnetic lenses, focused at the specimen surface and systematically scanned across the surface of a specimen. SEM never form a real image of the sample, but in the form

of a serial data stream. It is a result of the beam probe illuminating the sample one point at a time in a rectangular scanning pattern, with the strength of the secondary electrons generated from each point reflecting differences in the sample. Increased magnification is produced by decreasing the size of the area scanned. Depth of focus and resolution are influenced by the beam spot size, working distance, aperture size, etc. Electron beam shape, size and the position on the surface of specimen are controlled by lenses and coils [20].

In this work, microstructure information on metal alloy surface can be acquired, which provide qualitative carbon formation tendency and the morphology of metal oxide particles. The analyses were carried out at 5 or 10 kV accelerating voltage in vacuum conditions and different magnification was applied for each sample.

3.4.2 Raman Spectroscopy

Raman spectroscopy is a spectroscopic technique used to observe vibrational, rotational, and other low-frequency modes in a system, and it is commonly applied to provide a fingerprint of chemicals by which molecules can be identified. Raman effect occurs when electromagnetic radiation impinges on a molecule and interacts with the polarizable electron density and the bonds of the molecule in the phase (solid, liquid or gaseous) and environment in which the molecule finds itself. Photon interacts with molecule and scatters from it, different scattering process exist such as elastic scattering, called Rayleigh scattering, which is the dominant process (**Figure 3. 6**). The other process is inelastic, called Raman scattering, where nuclear motion is induced during the scattering process [21]. The laser light interacts with molecular vibrations, phonons or other excitations in the system, resulting in the energy of the laser photons being shifted up or down. The shift in energy gives information about the vibrational modes in the system. Since the vibrational information is specific to the chemical bonds and symmetry of molecules, Raman spectroscopy can be applied to identify molecules.
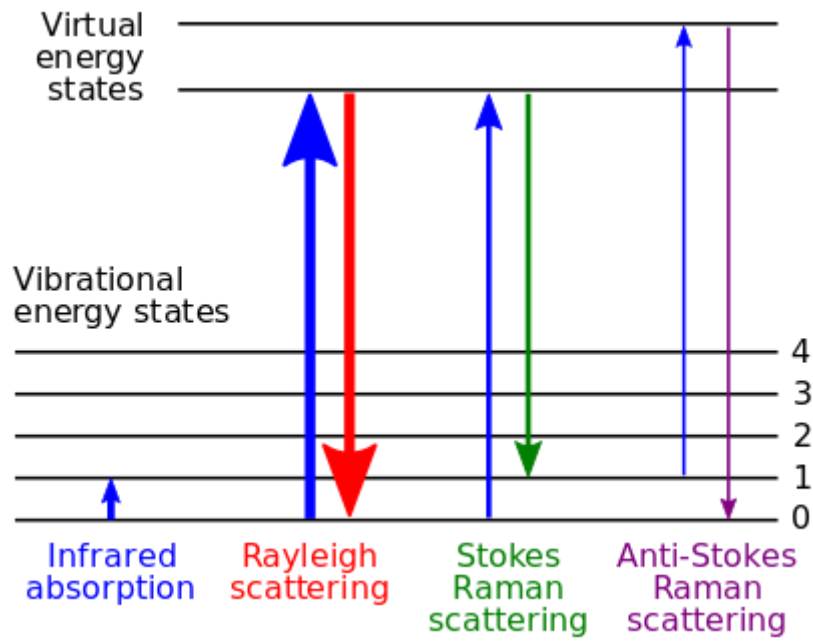
Figure 3. 6 Energy-level diagram showing the states involved in Raman spectra [21].

Raman spectroscopy is applied in this project to judge the composition changes on sample surface after CO exposure, especially recognizing newly-formed carbon and metal oxide.

Chapter 4. Results and Discussion

4.1 Inconel 601 samples

The variation of 601 coupons exposed to CO with different time is studied in this work. All pictures of samples shown in this chapter represents the surfaces of pre-oxidized Inconel 601 samples before or after the carburizing exposure for different time scale. The oxidation and CO exposure condition are listed in Chapter 3.

The SEM micrographs shown in **Figure 4. 1** are representative of the surface of observed for the pre-oxidized alloy Inconel 601 sample before exposure to the carburizing mixture. "Crystal-like" particles are identified on the surface, and the particles are dense but separated. Trace of polishing treatment, straight lines, were evident as well, which illustrates size of the particles is still relatively small.
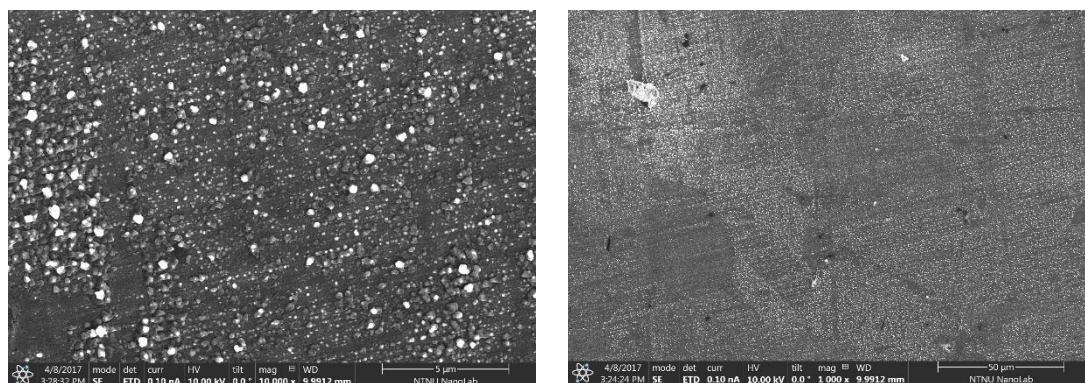
(a)   (b)

Figure 4. 1 Surface of pre-oxidized alloy Inconel 601 sample (a) magnification=1 k; (b) magnification=10k

Right after oxidation process, the samples were exposed to carburizing syngas mixture. The exposure was performed at $750℃$, at 20 bar under a $CO/H_2/CO_2/H_2O/Ar$ mixture of composition 20/25/15/10/30 (vol.%) for 10min, 30min, 1h, 5h, 10h and 20h, respectively. The nanostructure change and carbon formation on surfaces of the samples were further observed by SEM.

Figure 4. 2 shows the SEM micrographs of pre-oxidized Inconel 601 samples CO exposed for 10min, 30min and 1h. No carbon filament was found under SEM observation but particle size variation can be tracked. On the surface of sample CO exposed for 10 min, only tiny particles existed intensively, similar as pre-oxidized sample with CO exposure. Trace of surface polishing (straight lines) was still recognizable as well. When it comes to longer reaction time (30min), no significant changes showed comparing to the former sample but the average particle size increased. However, after 1h CO exposure, particles on the sample surface became not uniform, with larger particles growing inside grain boundary and smaller particles right along the grain boundary. The composition changes on surface were studied by Raman spectroscopy and these results will be shown later.

The results of SEM characterization of pre-oxidized Inconel 601 samples with 5h, 10h and 20h high pressure CO exposure are listed in **Figure 4. 3**. Clear carbon filament growth can be observed on the surface and an increasing trend of carbon filament can be observed with prolonged reaction time. When the alloy sample was exposed to CO for 5h, short and separated carbon nanofibers appears, with shape as sprouts that just have come out from soil. When the reaction time was prolonged (10h), carbon filaments grow longer, bending and twisting together, some carbon films have formed. When it comes to 20h, carbon film becomes denser and thicker, the size enlarges further as well.

As expected, carbon filaments grow longer and massive with longer CO exposure time on the samples, and, certainly, the largest amount carbon formation in our experiment was found in the experiment with longest reaction time (20h).
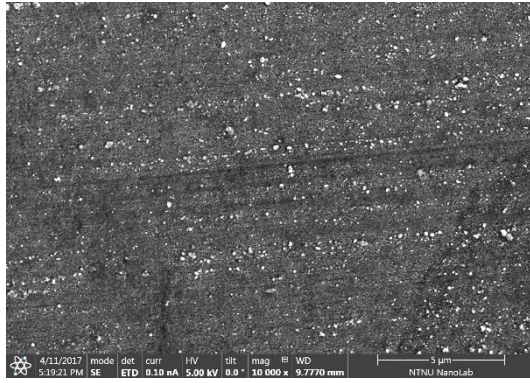
(a1)   (a2)
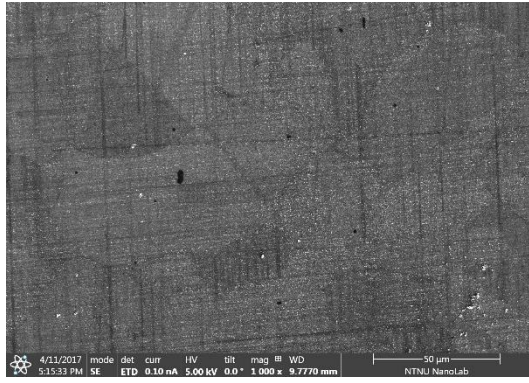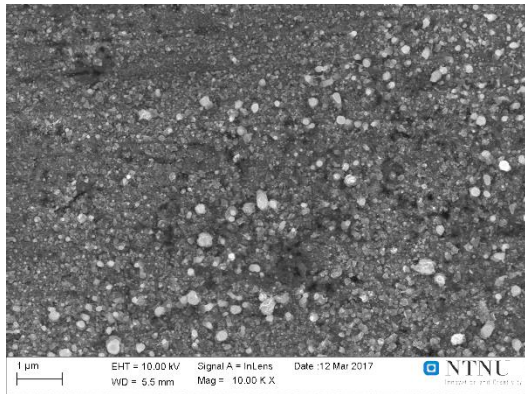
(b1)   (b2)
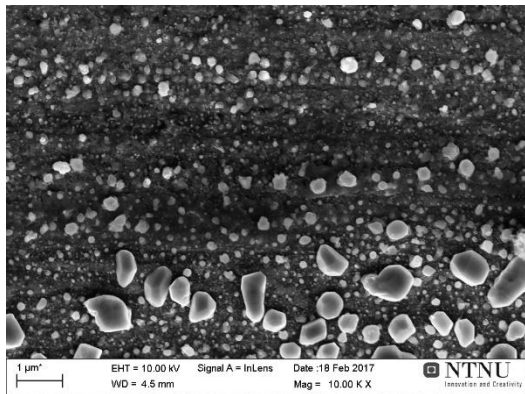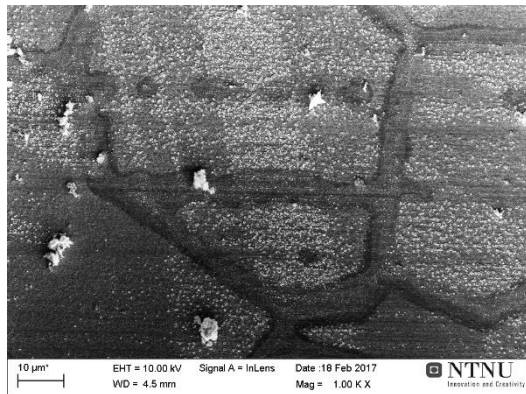
(c1)   (c2)

Figure 4. 2 SEM micrographs of CO exposed Inconel 601 samples. CO exposed for: (a1) and (a2) 10min; (b1) and (b2) 30min; (c1) and (c2) 1h.

(a1)

(a2)
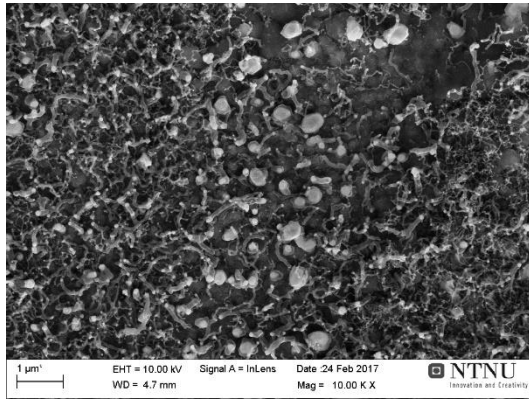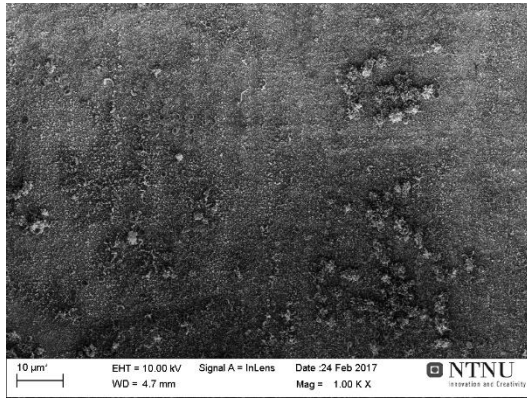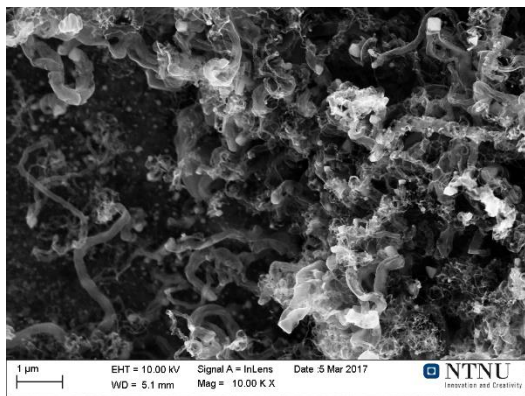
(b1)
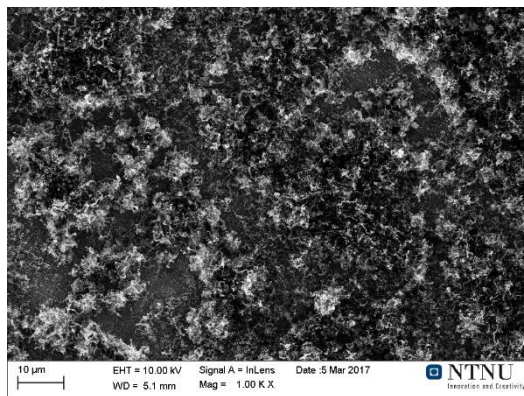
(b2)
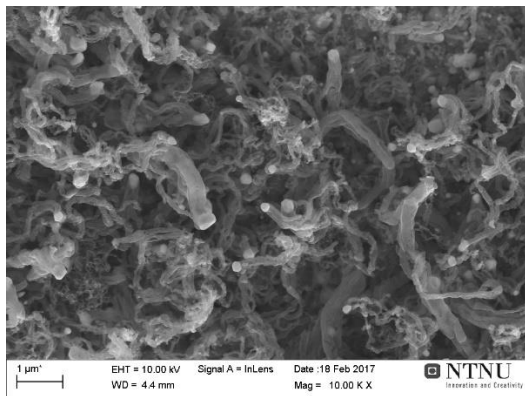
(c1)
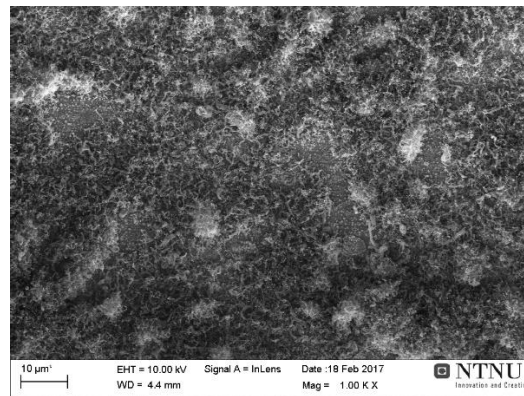
(c2)

Figure 4. 3 SEM micrographs of CO exposed Inconel 601 samples. CO exposed for: (a1) and (a2) 5h; (b1) and (b2) 10h; (c1) and (c2) 20h.

One interesting phenomenon identified on the sample CO exposed for 20h is that despite the large amount of carbon filaments that had been made, new carbon filaments formation was still proceeding. **Figure 4. 4** shows two newly-formed carbon filaments marked by arrows, on the top of which seemingly are the tips playing a role of catalysis.

Further element analysis via Energy-dispersive spectroscopy (EDS) was carried out later to identify the composition of the tip. When the mode of SEM transferred to EDS, however, the resolution ratio decreases significantly, leading to huge difficulties to select the exact tip point. And due to the working mechanism of EDS, the signal is not from the exact chosen point, but the area inside the bulk or deeper than the surface. Hence, the result was meaningless and not listed here. It is worth to conduct element analysis on the tip further with other methods, such as TEM.
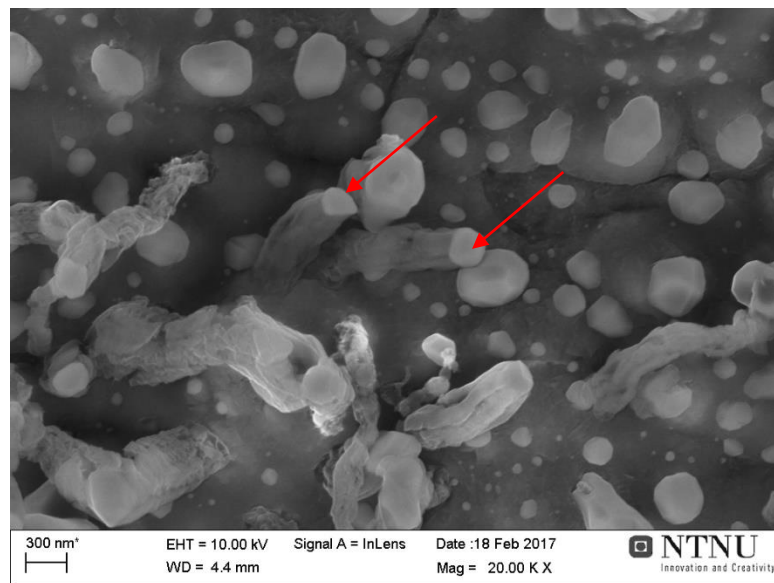

Figure 4. 4 New-formed carbon filaments on surface of sample after 20h CO exposure

In summary, according to SEM micrographs, pre-oxidized Inconel 601 alloy samples forms metal oxide particles. No visible carbon filament was observed on samples CO exposed less than 1h. Nevertheless, as the exposure time prolonging to about 5h, carbon filaments started to come out from the surface, and significantly increasing trend was observed.

The characteristics of the carbon formation were further investigated by Raman spectroscopy. The representative areas of each sample were chosen in the Raman spectrum acquisition.

Figure 4. 5 (a1) and (a2) exhibit the optical micrograph and spectrum of Inconel 601 sample exposed for 10min, respectively, which were acquired by Raman spectroscope. Straight lines on sample surface is the trace of polishing, and may imply that the oxide layer is thin. This is confirmed by color variation, which is caused by thin-film optic phenomenon. Daham [1] also confirmed that the thickness of oxide layer is less than 20nm with Auger electron spectroscopy. In terms of the spectrum, the absorption in the region 300-1000 cm^{-1} should be attributed to Cr_2O_3 (bands at 616, 553 and 353 cm^{-1} [22]), Fe oxide (band at 684.1 cm^{-1} [22]) Ni oxide (band at 530.8 cm^{-1} [23]). The main two carbon species bands in the spectra, the disordered (D) and graphite (G) peaks present at almost typical positions, around 1330 cm^{-1} and 1580 cm^{-1}, respectively. While the D band is so wide that overlaps to a large extent with the G band, which indicates highly disordered coke formed [24]. The D/G intensity ratio is relatively high, and no evident G' band (2685 cm^{-1}) reveals. Hence, it can be deduced there is some carbon formation on the sample, which is highly disordered and low crystallized, and it seems like glassy carbon according to the shape of spectra, however, invisible under SEM[10, 24].

Optical picture and Raman spectra of sample CO exposed for 30min are shown in **Figure 4. 5** (b1) and (b2). The spectra show similar shape as the one in **Figure 4. 5** (a2), which illustrates that the further formed carbon was still highly-disordered. While the width of D band decreases slightly, and a small peak reveal at G′ band position. The G' band is highly sensitive to the layer number of graphene [24], implying the formation of a small number of graphite carbon at this point. The spectra (**Figure 4. 5** c2) of sample exposed for 1h presents the more separated D band and G band, with D band becoming increasingly symmetric and narrow. A more evident G′ band can be seen as well. Therefore, it can be deduced that some amorphous or disordered carbon is synthesized first, which is not visible under SEM and quickly at the beginning of metal dusting

process, some carbon filament forms subsequently. Peaks representing metal oxide remain at the similar positions, which means little metal oxide transition occurred.

(a1) (a2)
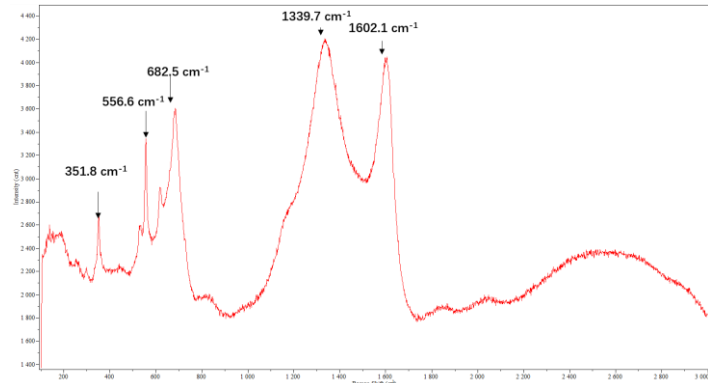
(b1) (b2)

(c1) (c2)

Figure 4. 5 Optical micrograph (magnification is 50 times) and corresponding Raman spectra of Inconel 601 sample after CO exposure for (a1) and (a2) 10min; (b1) and (b2) 30min; (c1) and (c2) 1h.
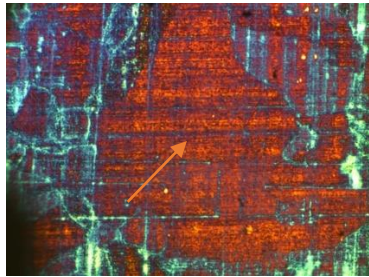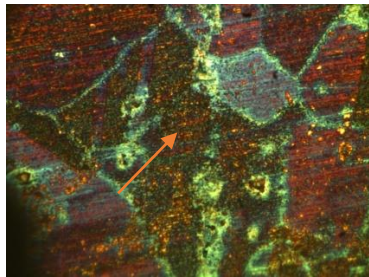
As listed in **Table 3. 2**, Inconel 601 is a type of Ni alloy with 13.3 wt% Fe content. According to the mechanism how iron catalyze carbon filament growth, there might be a small quantity of iron carbide formed on the surface. While feature peaks in iron carbide Raman spectrum are at the similar positions as D band and G band [25], signal of formed iron carbide was extremely possibly masked by these two bands. Consequently, it is hard to distinguish the existence of iron carbide merely through Raman spectrum. Other supported characterization method is necessary.

As mentioned above, carbon filaments were observed in case of 5h CO exposed sample under SEM observation. Some black areas revealed in the optical pictures of the sample (**Figure 4. 6**), and the corresponding Raman spectra presents strong carbon signal at D band and G band position. Intensity of peaks corresponding to carbon is much higher than intensity of metal oxide signal, indicating that signal of coke is much stronger than metal oxide or the coke layer is so thick that block the Raman signal from metal oxide underneath. And the intensities are also significantly higher than that in spectrum of samples exposed for less than 1h, showing that more carbon came out on the sample exposed for longer time(5h). The peaks become more symmetric and less overlapping as well. D′ band (shoulder at 1603 cm-1) and 2D band (about 26555 cm-1) are recognizable. Therefore, carbon made after 5h CO exposure is better crystallized than that formed on former samples, representative of the carbon filament structure [24].

The black area, representing coke formation, enlarged with exposure time expanding from 5h to 10h, 20h. This fits the situation observed by SEM that carbon filaments area extended with increasing CO exposure time. While Raman spectrums of samples exposed for 10h and 20h have nearly the same peaks' position and ratio between intensities of D band and G band, I_D/I_G, as the one for 5h. It illustrates that after the 5h CO exposure, carbon filament structure has developed well enough that disordered and crystallized have formed already. Length of the filaments grows further while carbon signal remains relatively stable.

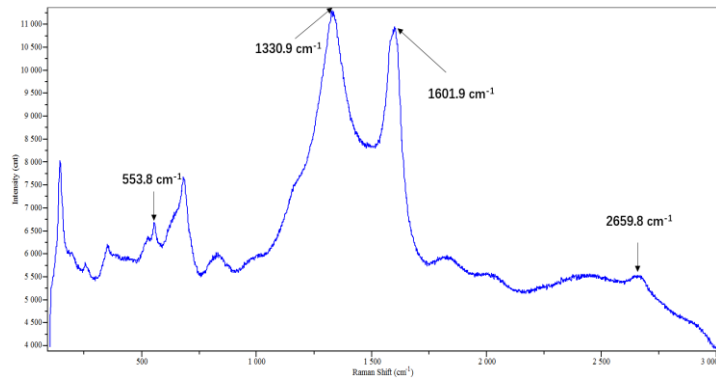(a1)   (a2)
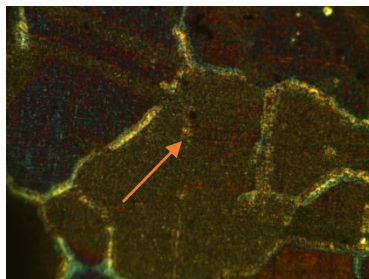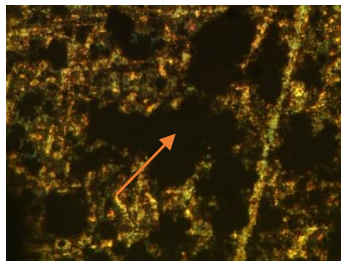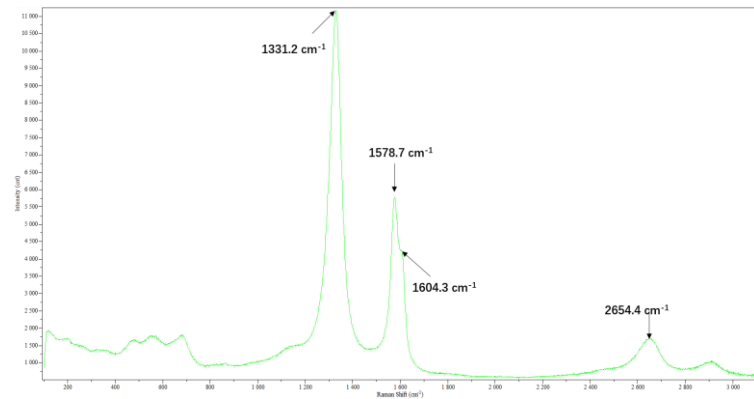

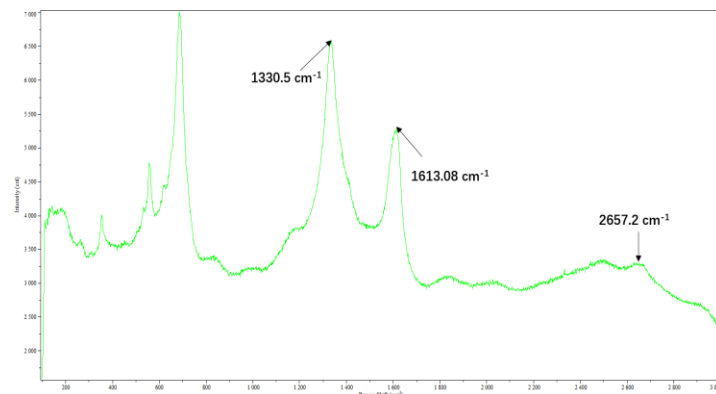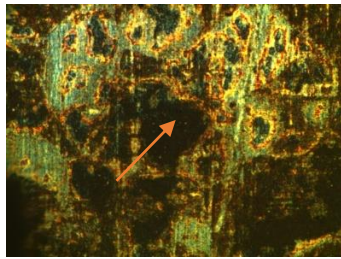(b1)   (b2)
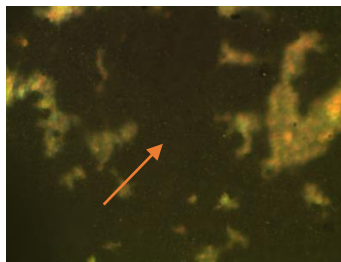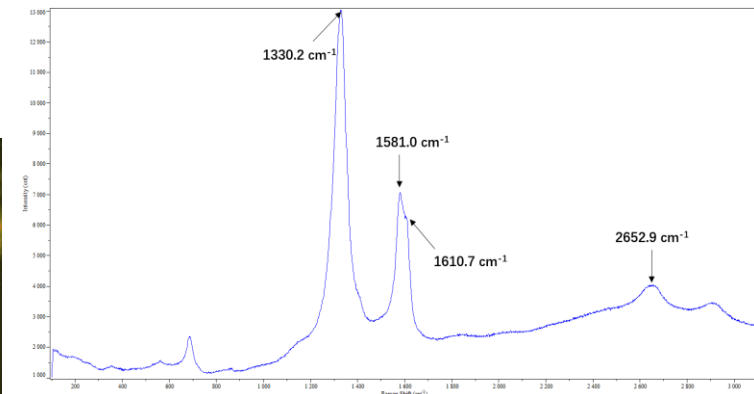
(c1)   (c2)

Figure 4. 6 Optical micrograph (magnification is 50 times) and corresponding Raman spectra of Inconel 601 sample after CO exposure for (a1) and (a2) 10min; (b1) and (b2) 30min; (c1) and (c2) 1h.

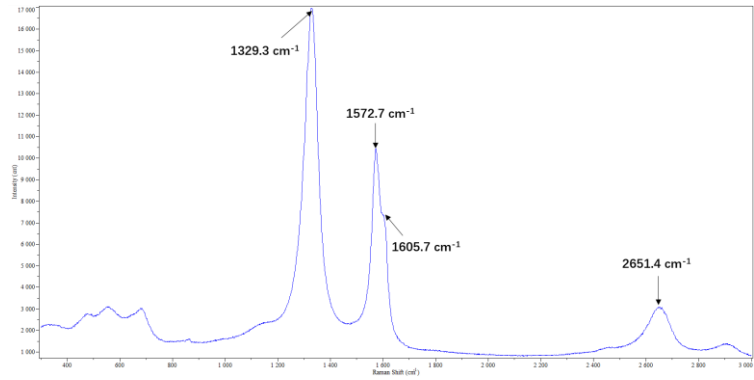As mentioned in Chapter 2, Z.Zeng and co-works proposed a metal dusting mechanism on Ni and Ni-alloy based on crystallization of carbon. Carbon transferred from gas phase to solid surface firstly forms poorly crystallized carbon. This description fulfilled

by samples exposed less than 1h. And after the deposited carbon diffusing through Ni matrix and precipitating at defects, better crystallization forms and grows, leading to breaks-up of the materials and further filament formation. This corresponds to the samples exposed for longer than 5h. Hence, results of exposure experiments on Inconel 601 samples satisfied the assumption came up with by Z.Zeng [10] to some degree.

Another point that should be considered about the carbon deposition, however, concerns to the first step in mechanism mentioned in Chapter 2. There was an oxide layer formed on Inconel 601 surface after the steam exposure. In principle, it has protective function against carbon deposition, while carbon deposition occurs on the layer and leads to carbon filaments growth subsequently. Two factors might contribute to the initial carbon deposition on the oxide layer, (1) The oxide layer is not uniform that some secondary phase exists, such as Ni, Fe, which could act as catalysts for carbon decomposition; (2) There are defects or cracks on the oxide layer, through which gas could flow underneath the layer and decomposes with help of alloy matrix. Therefore, further investigation, such as cross-section study, Auger electron spectroscopy, on the oxide layer formed on Inconel 601 is necessary, which may help to get a better understanding of metal dusting mechanism as well.

4.2 Incoloy 800 samples

The variation of Incoloy 800 coupons exposed to CO with different time is studied in the present work. All pictures of samples shown in this chapter represents the surfaces of pre-oxidized Incoloy 800 samples before or after the carburizing exposure for different time scale. The oxidation and CO exposure condition are listed in Chapter 3.

SEM micrographs of pre-oxidized sample are presented in **Figure 4. 7**. Small crystallite-like particles were formed, and more intensively in some areas. The parallel lines are the marks of polishing disposure before any treatment.
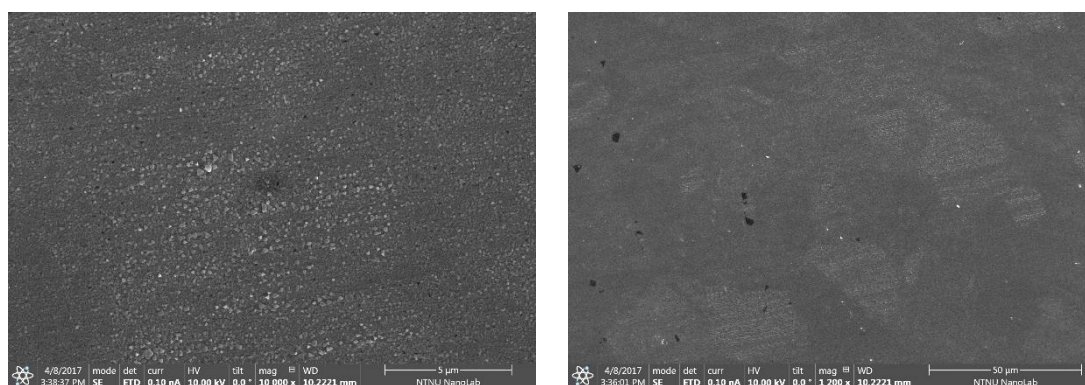
Figure 4. 7 Surface of pre-oxidized alloy Incoloy 800 sample (a) magnification=1.2 k; (b) magnification=10k

SEM micrographs of all pre-oxidized Incoloy 800 alloy samples exposed to CO for different time were listed in **Figure 4. 8**. All Incoloy 800 samples were pre-oxidized with 10% steam/ 90%Ar gas mixture at 1 bar for 6h. Right after oxidation process, the samples were exposed to carburizing syngas mixture. The exposure was performed at 750 ℃, at 20 bar under a $CO/H_2/CO_2/H_2O/Ar$ mixture of composition 20/25/15/10/30 (vol.%) for 10min, 30min, 1h, 5h, 10h and 20h, respectively. The nanostructure change and potential carbon formation on the samples' surfaces were further observed by SEM.

In general, no carbon formation on sample surfaces after exposure to the set condition was found, while clear nanostructure change can be observed. Surface of sample exposed for 10min (a1 and a2) had little change comparing to pre-oxidized Incoloy 800 sample. As the exposure time expanding to 30min (b1 and b2), a small inhomogeneous quantity of particles had been generated at the area inside the grain boundaries. After 1h exposure to the certain condition, the surface was totally covered by irregular particles (c1 and c2). Grain boundary was easy to recognize because of size of particles, with much smaller size at the grain boundary area. Newly-formed structure further developed with exposure time expanding to 5h (d1 and d2). Middle area within grain boundary swelled and generated stone-like structure, with much larger size and evident edges. The structure spread and develop uniformly, when it comes to 10h-exposed sample (e1 and e2), the surface was almost cover by the new structure except some grain boundary area, and further the whole surface was covered by the stone-like structure after 20h CO exposure (f1 and f2). The structure was further studied by Raman and verified to be spinel structure.

Characterization of composition transformation, especially for spinel structure, was further investigated by Raman spectroscopy. The representative areas of each sample were chosen in the Raman spectrum acquisition.

Figure 4. 9 list the Raman spectrum of pre-oxidized sample and optical picture of the corresponding point. Absorption at Raman shift 675.5 cm^{-1} and 546.8 cm^{-1} should be designated as a spinel solid solution $Fe_{3-x}Cr_xO_4$, with x around 1.2 [22]. Although there is color variation of some planes on the surface, compositions are relatively uniform.

(a1)

(a2)

(b1)

(b2)

(c1)

(c2)

39
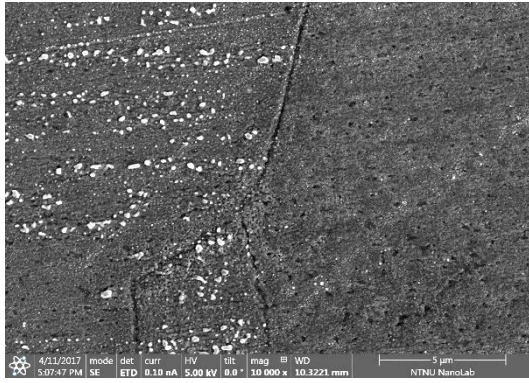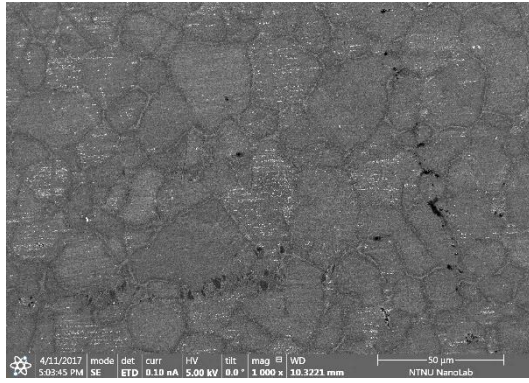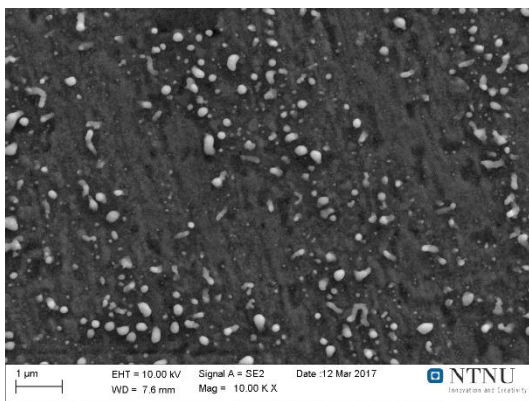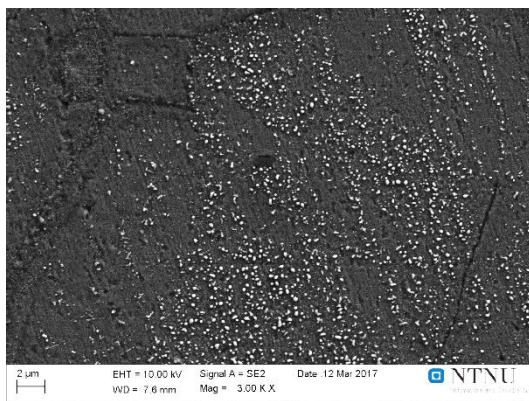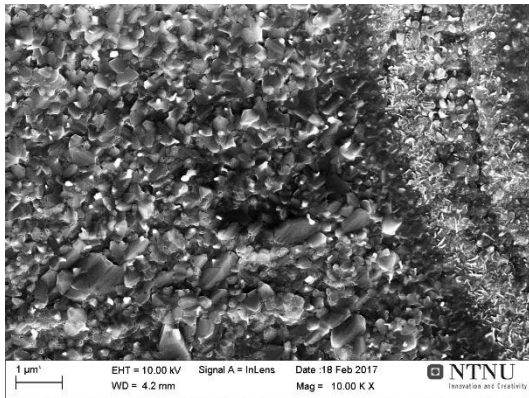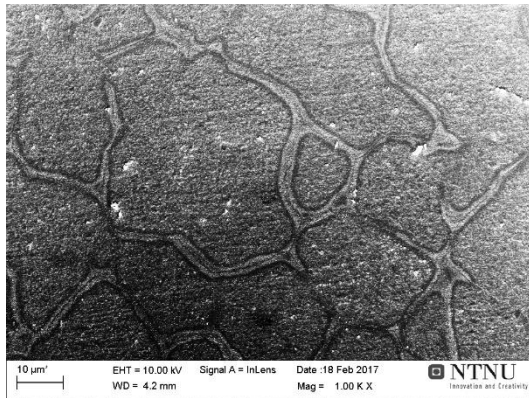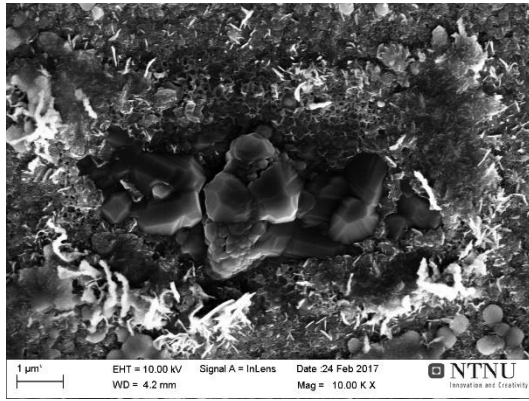
(d1)
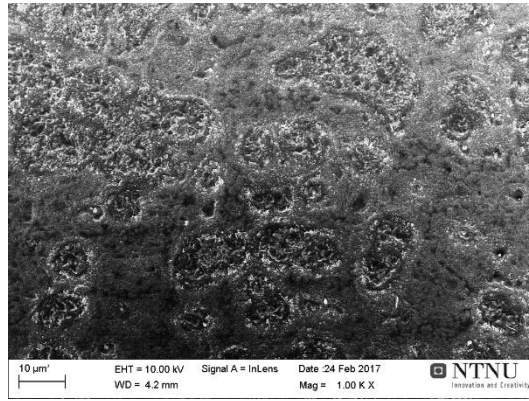
(d2)
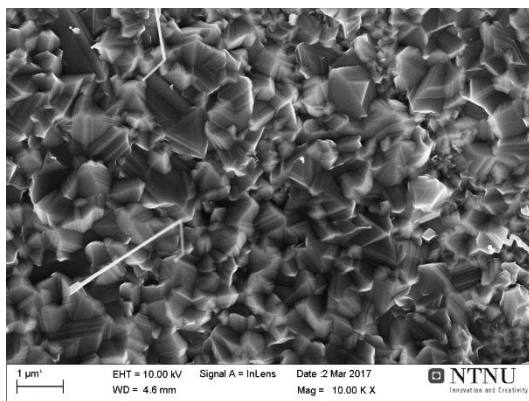
(e1)
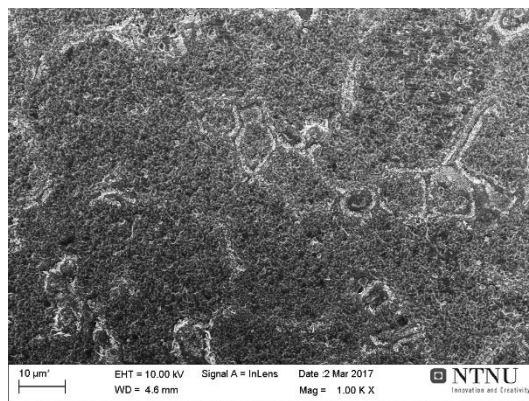
(e2)
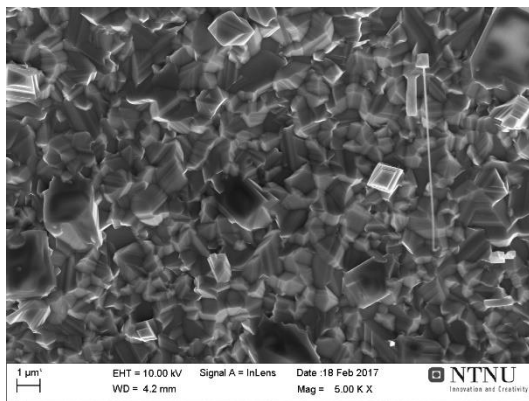
(f1)
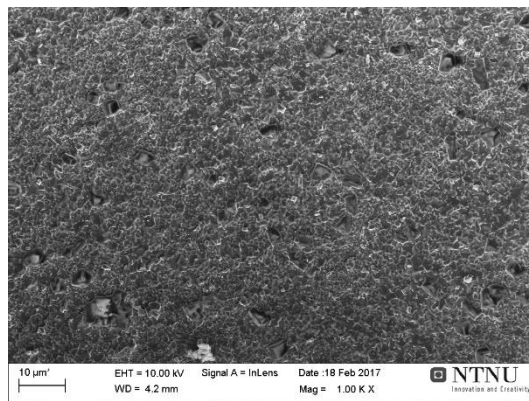
(f2)

Figure 4. 8 SEM micrographs of CO exposed Inconel 601 samples. CO exposed for: (a1) and (a2) 10min; (b1) and (b2) 30min; (c1) and (c2) 1h; (d1) and (d2) 5h; (e1) and (e2) 10h; (f1) and (f2) 20h

(a)   (b)

Figure 4. 9 Optical micrograph (magnification is 50 times) and corresponding Raman spectra of pre-oxidized Incoloy 800

All samples after CO exposure for 10min, 30min, 1h, 5h, 10h or 20h, exhibited Raman-scattering features mainly at wave range from 300~1000 cm^{-1}, which correspond to Fe oxide, Cr oxide and spinel compound [22]. While some sample presented weak signal at position representing coke formation, especially on sample with shorter exposure time. For example, Raman spectra of Incoloy 800 CO exposed for 30min is listed in **Figure 4. 10** (a), the typical carbon signal, D band at 1330 cm^{-1} and G band at 1580 cm^{-1} are clear. It might contribute to two factors: (1) Some metal oxides, i.e. Fe_2O_3, present peaks at similar position as D band for carbon in Raman spectrum [22], (2) Some carbon might form during cooling process, with system pressure declining dramatically and some CO remaining inside. The oxide layer formed under shorter CO exposure has many defects and cannot resist carbon formation well (discussed in detail later), and coke forms more easily under relatively lower pressure and lower temperature. This was confirmed by an additional experiment, that the 30min CO exposure experiment was repeated on Incoloy 800 sample, while remaining high pressure (20bar) during cooling process. As a result, no carbon signal came out in the Raman spectrum of this sample (**Figure 4. 10 b**). (3) There might be a slight amount of carbon formed during CO exposure, while it gasified later.

| (a) | (b) |
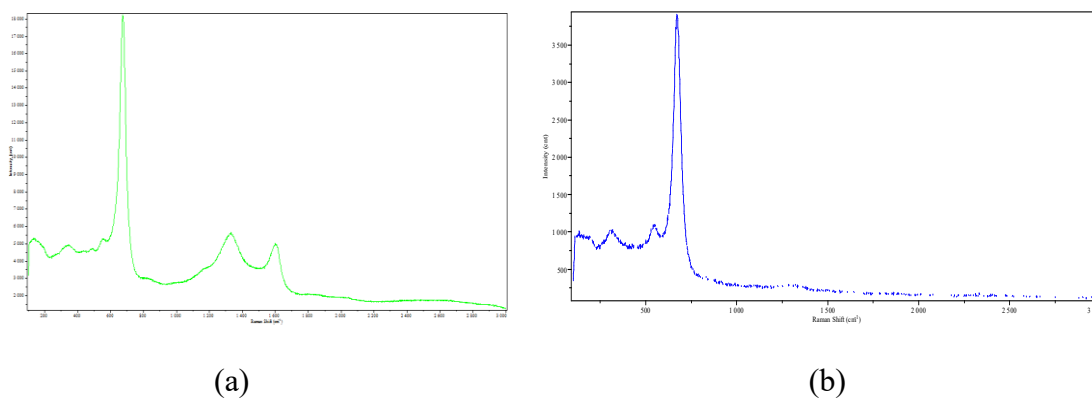
Figure 4. 10 Raman spectrums of samples with CO exposure for 30min; (a) the original experiment; (b) the repeated experiment

Optical picture and Raman spectrum of Incoloy 800 sample exposed for 10min are exhibited in **Figure 4. 11**. Comparing to **Figure 4. 9** (b), the feature peak, which has the highest intensity, shifts to a higher level at 682.07 cm^{-1}, which might be assigned to a new form of solid solution, $Fe_{2-x}Cr_xO_3$, with x approximately ranges 1.07~1.33 [23]. And two sharp peaks, at Raman shift 554 cm^{-1} and 352 cm^{-1} came out, which are all typical peaks' positions of Cr_2O_3. As described in Chapter 3, the sample was subjected to steam oxidation and CO exposure in a row, which means there was a stage that temperature and pressure increasing together. It normally lasted for 40min in the experiments. It has been proved that Fe and Cr are more sensitive to oxidation under elevating temperature [23]. And high temperature also boosts Cr diffusion from bulk to surface [9]. For Incoloy 800 sample CO exposed for 10min, the expose step (10min) is much shorter than the transferring step (40min), therefore, the ramping step posed larger impacts on the sample comparing to the CO exposure step. As a result, Fe and Cr on the sample surface were possibly further oxidized, from solid solution $Fe_{3-x}Cr_xO_4$ to solid solution $Fe_{2-x}Cr_xO_3$ and Cr enriched as well comparing with the pre-oxidized sample.

(a)   (b)

Figure 4. 11 Optical micrograph (magnification is 50 times) and corresponding Raman spectra of Incoloy 800 sample after CO exposure for 10min

Optical picture of sample surface CO exposed for 30min is shown in **Figure 4. 12** (a), with grain boundaries clearly recognizable. Point a, representing center area within grain boundary, exhibited Raman-scattering features mainly at 322.0 cm^{-1}, 549.7 cm^{-1}, and 673.7 cm^{-1} Figure **4. 12** b). The peaks' position, especially for the feature peak, transferred to low Raman shifts compared to the spectrum of 10min exposed sample (**Figure 4. 11** b). This reveals Fe containment increasing at the center area and might be caused by longer synthesis gas mixture exposure. When it comes to grain boundary area, point b, the feature peak shift to a higher position (**Figure 4. 12** b), indicating the higher Cr content and this is possibly due to higher Cr diffusion rate along the grain boundary [9,27].

Optical picture of sample surface CO exposed for 1h is shown in **Figure 4. 13** (a), with grain boundaries still clearly recognizable. Point a, representing center area within grain boundary, exhibited Raman-scattering features mainly at 313.3 cm^{-1}, 541.1 cm^{-1}, and a strongest feature at 670.8 cm^{-1}. When it comes to point b, grain boundary area, the peaks shifted to high position at 304.2 cm^{-1}, 539.3 cm^{-1}, and 667.2 cm^{-1}.

(a)	(b)

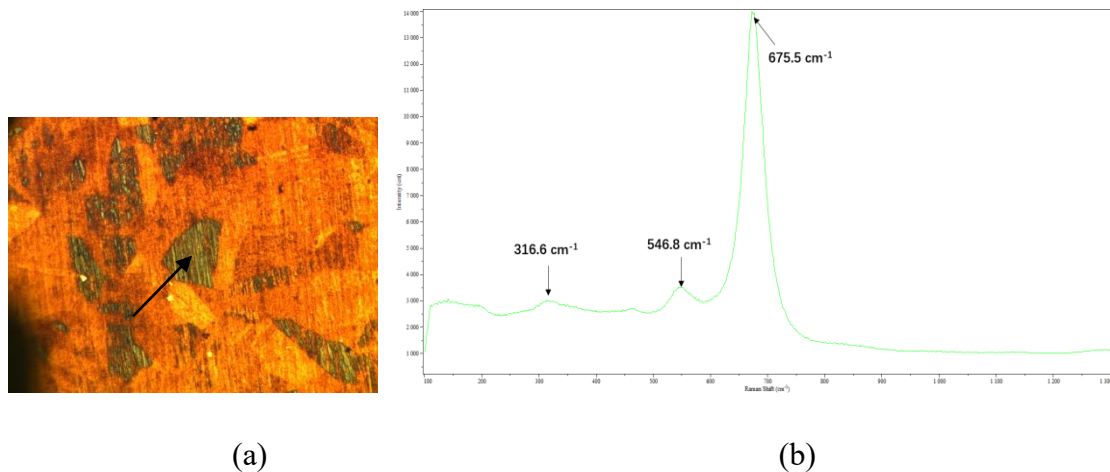**Figure 4. 12 Optical micrograph (magnification is 50 times) and corresponding Raman spectra of Incoloy 800 sample after CO exposure for 30min, (a) center area; (b) grain boundary**

Raman mapping was carried out to provide more direct and distinct comparison of the composition difference at grain boundary area and within the grain boundary center. Raman mapping tests several points in a chosen area or along a chosen line one by one within a short time period, and exhibits the spectrums of the chosen points together. The chosen line and acquired spectrums on the sample are shown in **Figure 4. 14**. Four points on the chosen line were characterized, of which the third one is on the grain boundary and the others at the center of grain. Spectrums for point 1, 2 and 4 have almost the same appearance expect the intensity variation. It should be due to roughness of the surface impact focusing on the point. While spectrum of point 3 present a small sharp peak at about 555 cm^{-1}, illustrating higher content of Cr at grain boundary.

(a)   (b)

Figure 4. 13 Optical micrograph (magnification is 50 times) and corresponding Raman spectra of Incoloy 800 sample after CO exposure for 1h, (a) center area; (b) grain boundary

Figure 4. 14 Optical micrograph (magnification is 50 times) of Raman mapping area and corresponding Raman spectrums of Incoloy 800 sample after CO exposure for 1h

When it comes to alloy sample with 5h CO exposure, evident surface nanostructure change occurred comparing to samples exposed for 1h according SEM observation. In the optical picture, grain center area became darker due to new structure formed (**Figure 4. 15** a). In the spectra (**Figure 4. 15** b), the feature peak shifts to a lower position comparing to spectra **Figure 4. 13** (b), and it indicates the increasing content of Cr of the solid solution. Similar as sample exposed to 1h, a unique peak presents at position about 555 cm^{-1} in the spectra corresponding to grain boundary area, which is assigned to Cr_2O_3 [22]

Result of Raman mapping confirms the conclusion above (**Figure 4. 16**). Four points were tested along the selected line, with the third one was on the grain boundary and the others within the center grain area. Spectra of the third point shows different feature from the other ones'. The highest peak was located at a higher position, and the peak at about 555 cm^{-1} occurred as well.

(a)   (b)
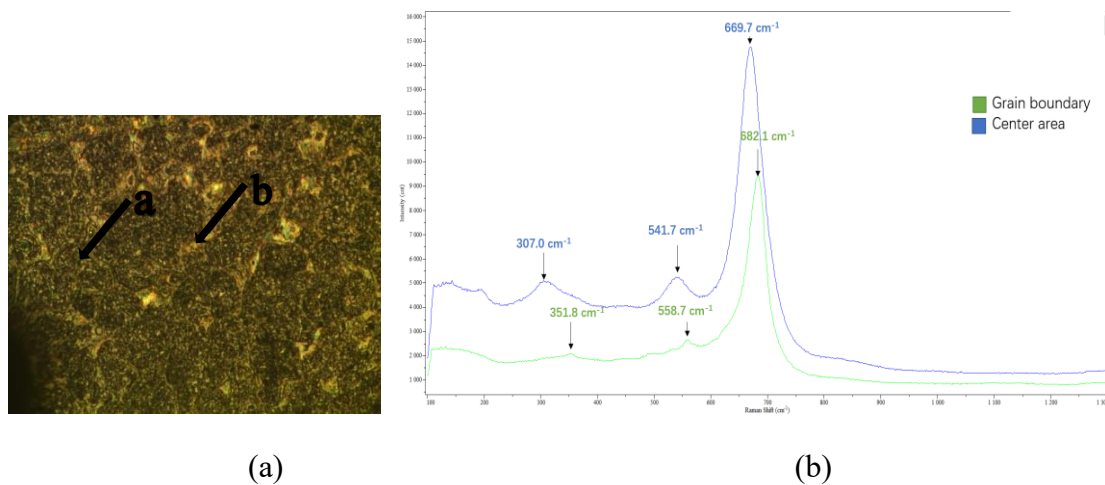
Figure 4. 15 Optical micrograph (magnification is 50 times) and corresponding Raman spectra of Incoloy 800 sample after CO exposure for 5h, (a) center area; (b) grain boundary
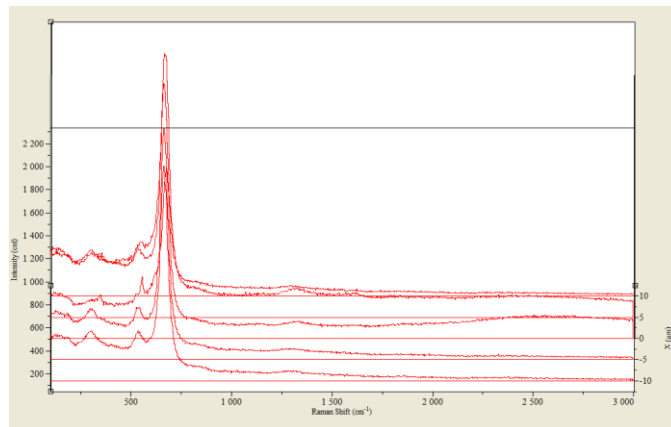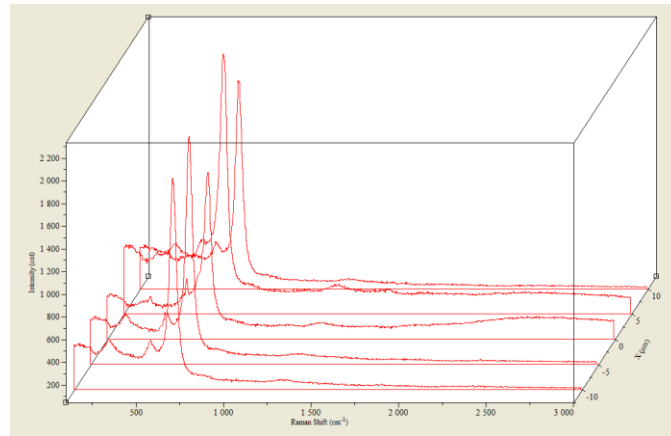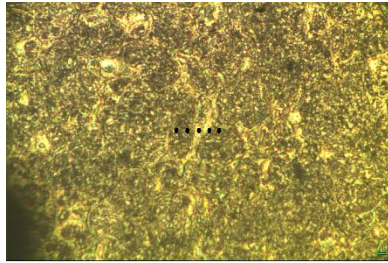
Figure 4. 16 Optical micrograph (magnification is 50 times) of Raman mapping area and corresponding Raman spectrums of Incoloy 800 sample after CO exposure for 5h

Figure 4. 17 shows the optical micrograph of the sample surface after 10h CO exposure and Raman spectrums of two chosen points within the region. The optical micrograph matched surface appearance observed by SEM, with the vast majority of area cover by spinel structure and some grain boundary area revealed. The absorption at positions 307.0 cm^{-1}, 539.5 cm^{-1} and 667.6 cm^{-1} in spectrum representing center area (point a) may be attributed to spinel solid solution $Fe_{2-x}Cr_xO_3$, with x at range of 0.27~0.53 [22], which fulfills the nanostructure of the point at center of the grain boundary observed via SEM. And spectrum of point b, corresponding to grain boundary, the highest shifted to slightly higher position, 686.8 cm^{-1},
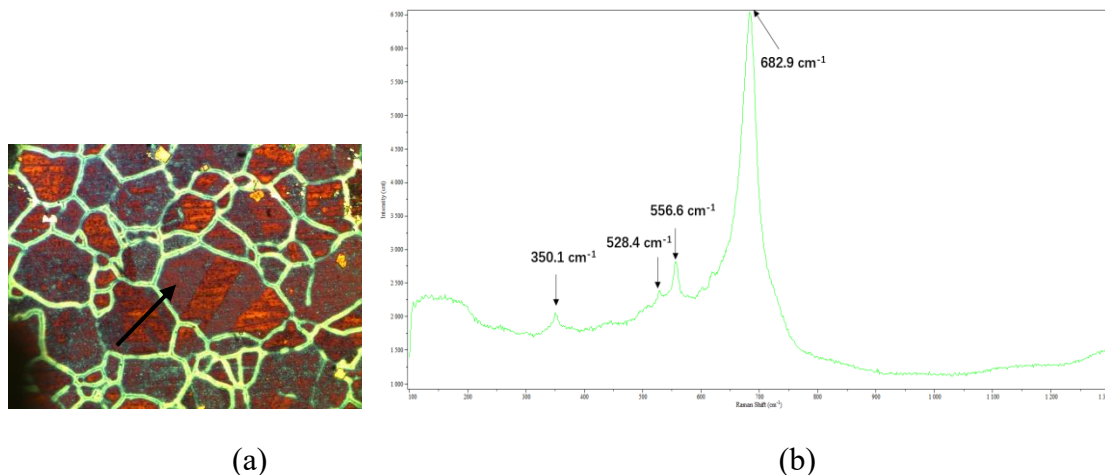
(a)   (b)
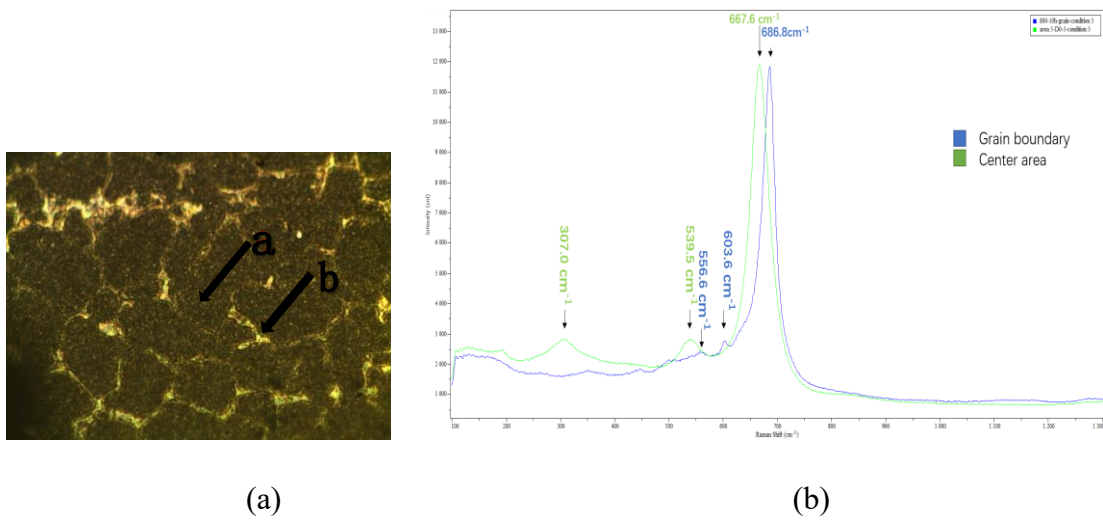
Figure 4. 17 Optical micrograph (magnification is 50 times) and corresponding Raman spectra of Incoloy 800 sample after CO exposure for 10h

Picture acquired with microscope using white light implies the uniformity of sample surface structure after 20h CO exposure (**Figure 4. 18** a). **Figure 4. 18** (b) shows the Raman spectrum and shows quite similar peak positions and intensities as spectrum **Figure 4. 17** (b). This corresponds to situation that the nanostructure of the sample observed by SEM that compounds on sample CO exposed for 20h is the same as compounds at the center area of sample CO exposed for 10h. The uniformity was further testified by Raman mapping. A random line was selected and points on the line was investigated by Raman spectroscope. The spectrums of each points are listed in **Figure 4. 19**, and it can be seen that all spectrums have nearly the same peaks' position and similar peaks' intensities.
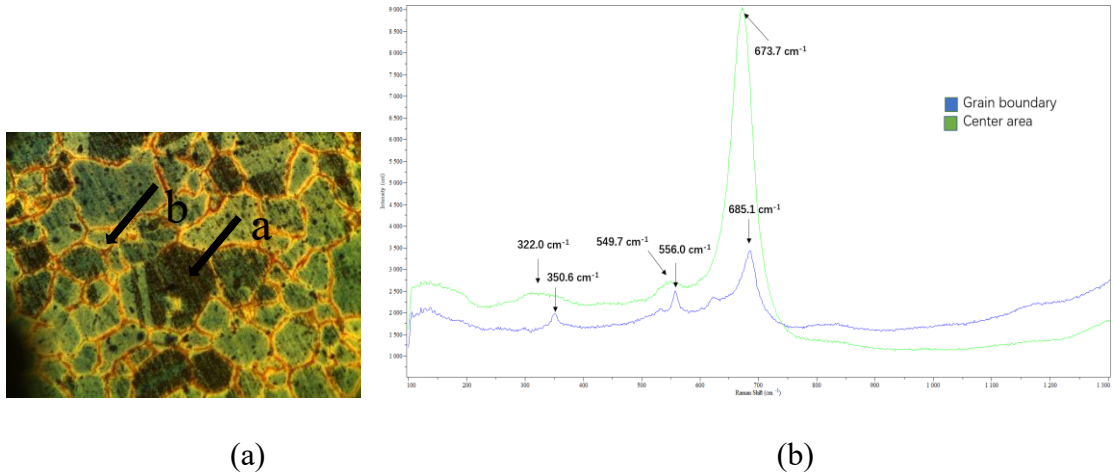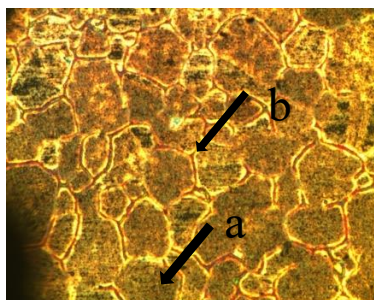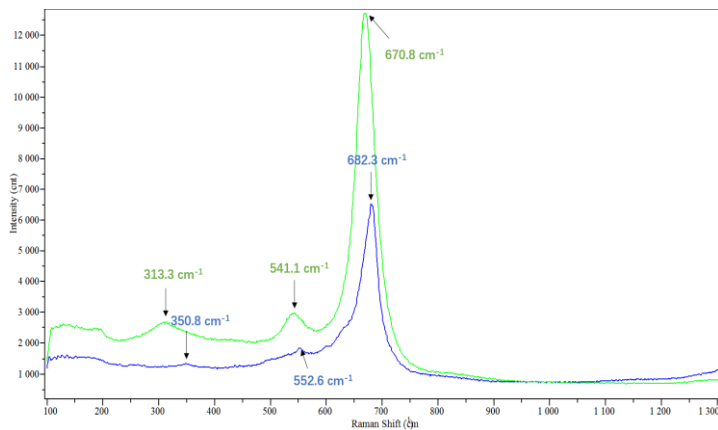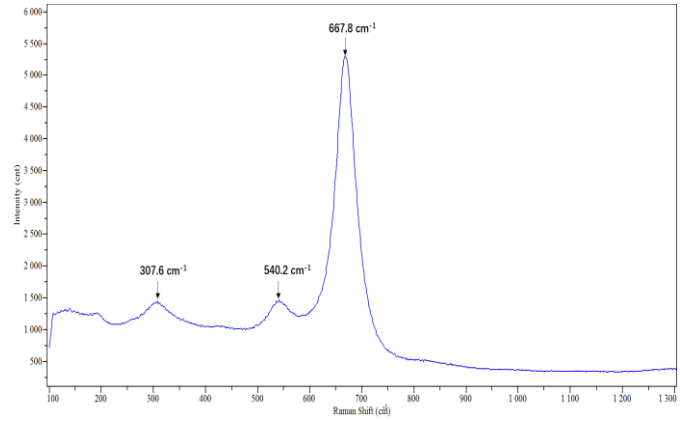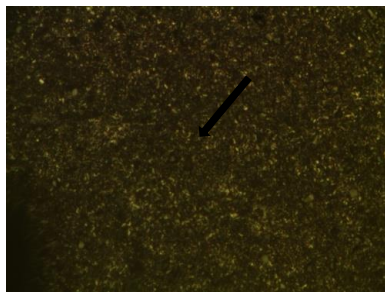
(a)   (b)

Figure 4. 18 Optical micrograph (magnification is 50 times) and corresponding Raman spectra of Incoloy 800 sample after CO exposure for 20h
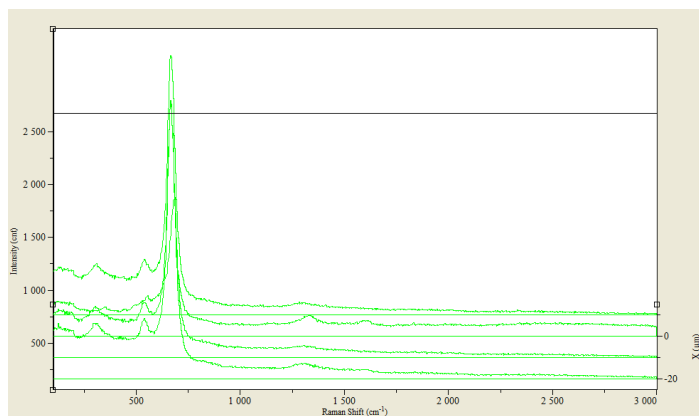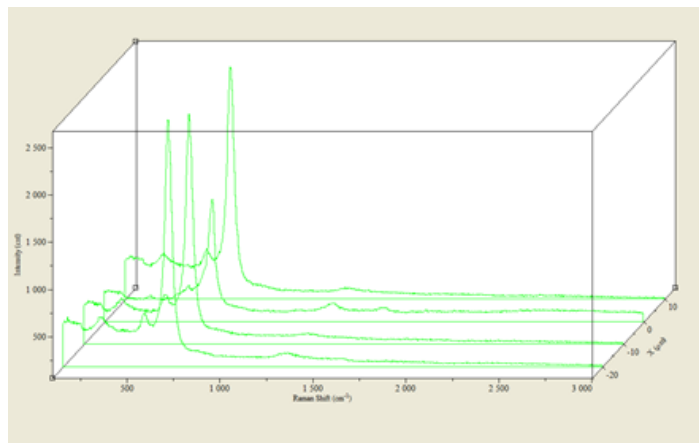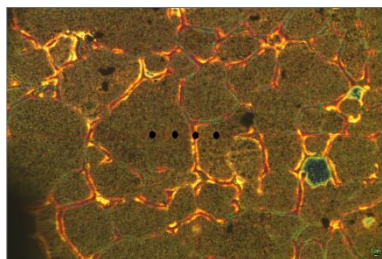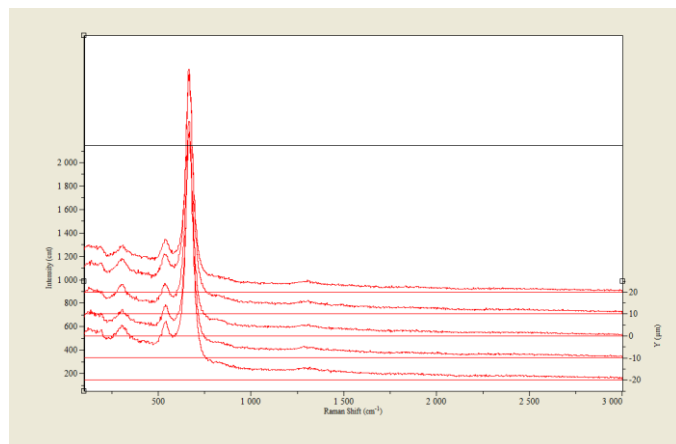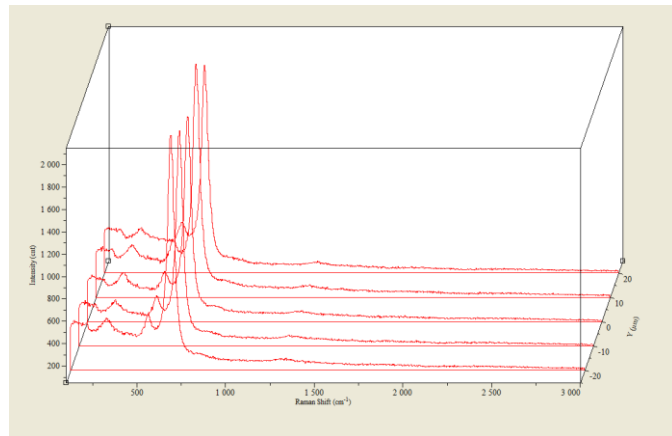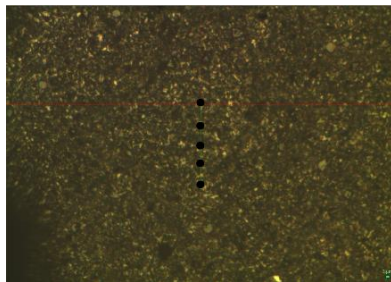

Figure 4. 19 Optical micrograph (magnification is 50 times) of Raman mapping area and corresponding Raman spectrums of Incoloy 800 sample after CO exposure for 20h

49

SEM micrographs and Raman spectrums indicate the composition variation on pre-oxidized Incoloy 800 alloy sample after CO exposure with different time under high pressure. After 10min CO exposure, the nanostructure only changes slightly, but composition is affected by heating and pressurized step. As a result, the solid solution $Fe_{3-x}Cr_xO_4$ formed during steam oxidation is further oxidized to solid solution $Fe_{2-x}Cr_xO_3$. When the exposure time expands to 30min, CO exposure influence reveals that Fe content at the center area increases. With exposure time prolonging to 1h, newly-formed particles arise and nearly cover the whole surface. Spinel structure begin to develop from the center area within grain boundary and spread further under longer exposure (5h). After 10h CO exposure, the spinel structure has covered a majority of surface, merely with grain boundary area left. The spinel structure was approved to be solid solution $Fe_{2-x}Cr_xO_3$ (x ranges from 0.27~0.53), while composition at grain boundary has higher Cr content. After 20h CO exposure, the spinel develops uniformly. And the peaks' positions in the spectrums shift to lower direction with exposure time prolonging (682.9 cm^{-1} to 667.8 cm^{-1} from 10min to 20h), and it illustrates that Fe content continuously increasing at the center area, however, without any carbon or carbide formation.

Nanostructure difference is evident between areas at center of grain and grain boundaries, and Cr content is higher at the grain boundary area. This confirms that Cr diffuses faster along with grain boundary.

Incoloy 800 has good metal dusting resistance under environment with relatively low carbon activity (a_c). The oxide layer further develops under the condition and play a role to separate gas phase and alloy bulk underneath. The resistance property of this oxide layer under more violent metal dusting environment were testified by Guo X. et al. Two experiments were conducted: (1) Prolonging experiment time under the same condition by expanding reaction time to 40h without adjusting other parameters. The

oxide layer showed promising resistance as well that no indicated carbon filament formation on sample surface as examined by SEM and Raman spectroscopy. Hence, it is further verified that the oxide layer formed on Incoloy 800 is able to prevent the alloy from metal dusting corrosion under environment with relatively low carbon activity; (2) Utilizing metal dusting environment with infinite carbon activity ($a_c \gg 1$). Experiment on the sample with 20h CO exposure was conducted under a more violent metal dusting environment ($a_c \gg 1$), at 550°C, at 1 bar in 100 Nml/min with 10% CO-Ar gas (carbon activity: $ac \gg 1$) for 1 h to 20 h. A great amount of carbon formed on the sample surface. When the oxide layer exposed to complete reduction atmosphere (CO and Ar without steam), it cannot continuously retain to be intact and act protective role well, which illustrates that the oxide layer is not strong enough to protect the alloy under severe metal dusting condition, especially atmosphere without steam, i.e. oxidation condition.

4.3 Comparison of Inconel 601 and Incoloy 800

As mentioned above, Inconel 601 and Incoloy 800 samples both went through steam oxidation and different time CO exposure, at 750 °C, at 20 bar in gas flow with a $CO/H_2/CO_2/H_2O/Ar$ gas mixture of composition 20/25/15/10/30 (vol.%) for 10min to 20 h. Inconel 601 performs poorly, with carbon deposition occurring from quite early moment, and carbon filaments arose after 5h or longer time CO exposure. No carbon filament was observed on Incoloy 800 surface after CO exposure and no carbon signal was detected via Raman spectroscopy as well. Incoloy 800 exhibits superior metal dusting resistance than Inconel 601 under the environment used in this paper. This might be due to the difference between the oxide layers on the sample surface. Both the two alloy materials form oxide layer after steam oxidation. While the layer on Incoloy 800 could further develop to a dense and uniform layer; Inconel might have separated phase that catalyzes carbon deposition, leading to easily gas flow penetration from gas phase to metal matrix and, furthermore, metal dusting corrosion.

To get a better insight into the reason of performance gap between Inconel 601 and Incoloy 800, more efforts should be paid. For example, experiments with different oxidation condition need to be carried out on the two types of alloy materials, and more characterization methods should be considered as well.

Chapter 5 Conclusions

The initial stage of metal dusting on surfaces of alloy samples under high pressure were investigated in this paper.

Two types of alloy, Inconel 601 and Incoloy 800, were selected for the experiments. The samples were polished first, and pre-oxidized under for 6 h at 540 °C, at 1 bar under 10% steam-Ar gas mixture flowing at a rate of 100 Nml/min. Consequently, CO exposure experiments with the pre-treated sample were conducted at 750 °C, at 20 bar in 100Nml/min gas flow with a $CO/H_2/CO_2/H_2O/Ar$ gas mixture of composition 20/25/15/10/30 (vol.%) for 10min to 20 h.

Characterization methods, scanning electron microscopy and Raman spectroscopy, were utilized to observe and study the nanostructure or composition changes on alloy sample surfaces.

5.1 Inconel 601 samples

Inconel 601 exhibits poor metal dusting corrosion resistance under the experiment condition that evident carbon filaments forms on the sample surfaces under SEM observation when the exposure time is longer than 5 hours, and more carbon were produced with longer CO exposure time. Newly-formed carbon filaments continue to arise even a large number of carbon filaments have occurred (sample with 20h CO exposure). When all samples were studied via Raman spectroscopy, it was discovered that carbon deposition start really early, even on sample CO exposed for 10min, with disordered carbon firstly emerges on the alloy surface and well crystalized carbon forms as exposure time expanding.

5.2 Incoloy 800 samples

Inconel 800 exhibits comprising metal dusting corrosion resistance under the experiment condition that no carbon filament was observed visually or under SEM lens, even the sample with longest exposure time (20h). There was no carbon signal coming out from samples against Raman spectroscopy test as well.

Spinel structure, $Fe_{3-x}Cr_xO_4$, forms firstly right after steam oxidation. While during the ramping stage from steam oxidation to CO exposure, the spinel solid solution is further oxidized to another form, $Fe_{2-x}Cr_xO_3$. With exposure time expanding, Fe content at the center area within grain boundary decreases slightly (x from around 1.07 to less than 0.53), and an oxide layer arises from the middle area, developing further until all surface are covered by it. The layer plays good protection role against the metal dusting environment utilized in this paper, while it may lose the protective function when it faces more violent metal dusting condition.

Chapter 6 Further work

- **Utilization of more characterization methods**

The newly-formed carbon filament listed in Chapter 4.1 is worth to be analyzed by more characterization methods, such as EDS or other composition analysis methods, to investigate where is the activated site easily "affected" by carbon formation. And combination of multiple characterizations can help to increase the accuracy and provide more evidence or information.

- **Cross-section observation**

In this report, most of the efforts was paid to analyze how sample surface changes after CO exposure, while inner changes were relatively ignored. Through cross section study, it can be seen that diffusion of elements from alloy surface to bulk or opposite direction, which provides some possible explanation for the structure or composition transition on surface.

- **Investigation of the exact moment that carbon filament comes out**

On the surfaces of the Inconel 601 samples exposed less than 1 hour, no carbon filament is observed but carbon formation occurs. However, carbon filaments had formed on Inconel 601 sample CO exposed for 5h. It can be deduced that carbon filament came out at an exact moment between 1h and 5h exposure time. Studying the exact moment and sites that carbon filaments start to grow is meaningful to understand the carbon growth mechanism and create methods to prevent it.

- **Methods to build batter protection oxide layer on Inconel 800 alloy**

Since the formed oxide layer can function as protective layer under the carburizing environment applied in this paper, it is meaningful to find the methods, such as utilizing different oxidization conditions, promote the layer and make it more efficient under more severe metal dusting environment.

Reference

1. Gunawardana, P., *Carbon formation phenomena and the initial stage of metal dusting corrosion–an experimental investigation*. Doctoral thesis, Norwegian University of Science and Technology (NTNU), Trondheim, Norway, 2014.

2. Szakálos, P., *Mechanisms of metal dusting.* Doctoral thesis, Royal Institute of Technology (KTH), Stockholm, Sweden, 2004.

3. Grabke, H., C. Bracho‐Troconis, and E. Müller‐Lorenz, *Metal dusting of low alloy steels*. Materials and Corrosion, 1994. 45(4): p. 215-221.

4. Zeng, K.N.a.Z*., Development of Materials Resistant to Metal Dusting Degradation*. Annual Report, Energy Technology Division, Argonne National Laboratory, 2006.

5. Guo X, Gunawardana P, Chen D, et al. *Investigation of Metal Dusting Corrosion Process over UNS N08800 Alloy[C]*//CORROSION 2017. NACE International, 2017.

6. Grabke, H., et al., *Metal dusting of nickel‐base alloys*. Materials and Corrosion, 1996.47(9): p. 495-504.

7. Grabke, H. J.; Krajak, R.; Nava Paz, J. C., *On the mechanism of catastrophic carburization: 'metal dusting'*. Corros. Sci. 1993, 35, (5–8), 1141-1150.

8. Grabke, H., *Thermodynamics, mechanisms and kinetics of metal dusting*. Materials and Corrosion, 1998. 49(5): p. 303-308.

9. Grabke, H. J., *Metal dusting.* Mater. Corros. 2003, 54, (10), 736-746.

10. Zeng, Z.; Natesan, K*., Relationship of carbon crystallization to the metaldusting mechanism of nickel*. Chem. Mater. 2003, 15, (4), 872-878.

11. Agüero A, Gutiérrez M, Korcakova L, et al. *Metal dusting protective coatings. a literature review[J]*. Oxidation of metals, 2011, 76(1-2): 23-42.

12. P. Abbott, J. Edwards, J. B. Crewdson, and M. Fowles. *Metal passivation in a heat exchange reformer*. Patent, WO 03/051771 (2003).

13. C. Rosado, M. Schütze, *Protective behaviour of newly developed coatings against metal dusting,* Mater. Corros. 54 (2003) 831–854.

14. Kirchheiner, R.; Soler, J. L. J., *Correlation of oxidation, carburization and metal dusting; "Controlling corrosion by corrosion".* In CORROSION 2001, NACE International: Houston, TX, 2001; Vol. Paper No.01374.

15. C.G.M. Hermse, H. van Wortel, *Applicability of coatings to control metal dusting*, NACE Corrosion 2009 (2009).

16. Madloch S, Galetz M C, Geers C, et al. *Development of a metal dusting resistant functional coating by Sn and Al pack cementation[J]*. Surface and Coatings Technology, 2016, 299: 29-36.

17. Alvarez J, Melo D, Salas O, et al. *Protective coatings against metal dusting*[J]. Surface and Coatings Technology, 2008, 203(5): 422-426.

18. Special Metals, *Product handbook of high-performance nickel alloys*. Retrieved May 12, 2017, from:

    http://www.specialmetals.com/files/PCC-8064-SM-AlloyHandbook_v04.pdf.

19. *Scanning electron microscope*, Retrieved December 13, 2016, from:

    https://en.wikipedia.org/wiki/Scanning_electron_microscope

20. *MyScope, SEM*. Retrieved May 12, 2017, from

    http://ammrf.org.au/myscope/sem/practice/principles/layout.php#detail

21. *Raman spectroscopy.* Retrieved May 12, 2017, from

    https://en.wikipedia.org/wiki/Raman_spectroscopy

22. McCarty K F, Boehme D R. *A Raman study of the systems Fe3− xCrxO4 and Fe2− xCrxO3[J]*. Journal of solid state chemistry, 1989, 79(1): 19-27.

23. Renusch D, Veal B, Natesan K, et al. *Transient oxidation in Fe-Cr-Ni alloys: A Raman-scattering study[J]*. Oxidation of metals, 1996, 46(5): 365-381.

24. Zeng Z, Natesan K, Maroni V A. *Investigation of metal-dusting mechanism in Fe-base alloys using raman Spectroscopy, X-Ray diffraction, and electron microscopy[J]*. Oxidation of metals, 2002, 58(1-2): 147-170.

25. 20. Y.-H. Lin, C.-Y. Yang, S.-F. Lin, G.-R. Lin, *Triturating versatile carbon materials as saturable absorptive nano powders for ultrafast pulsating of erbium-doped fiber lasers*, Optical Materials Express 5, 2 (2015): p. 236.

26. Lamim T S, Benardelli E A, Binder C, et al. *Plasma carburizing of sintered pure iron at low temperature[J]*. Materials Research, 2015, 18(2): 320-327.

27. Grabke H J, Muller-Lorenz E M, Strauss S, et al. *Effects of grain size, cold working, and surface finish on the metal-dusting resistance of steels[J]*. Oxidation of Metals, 1998, 50(3): 241-254.

Appendix

Appendix A: Detailed Setup
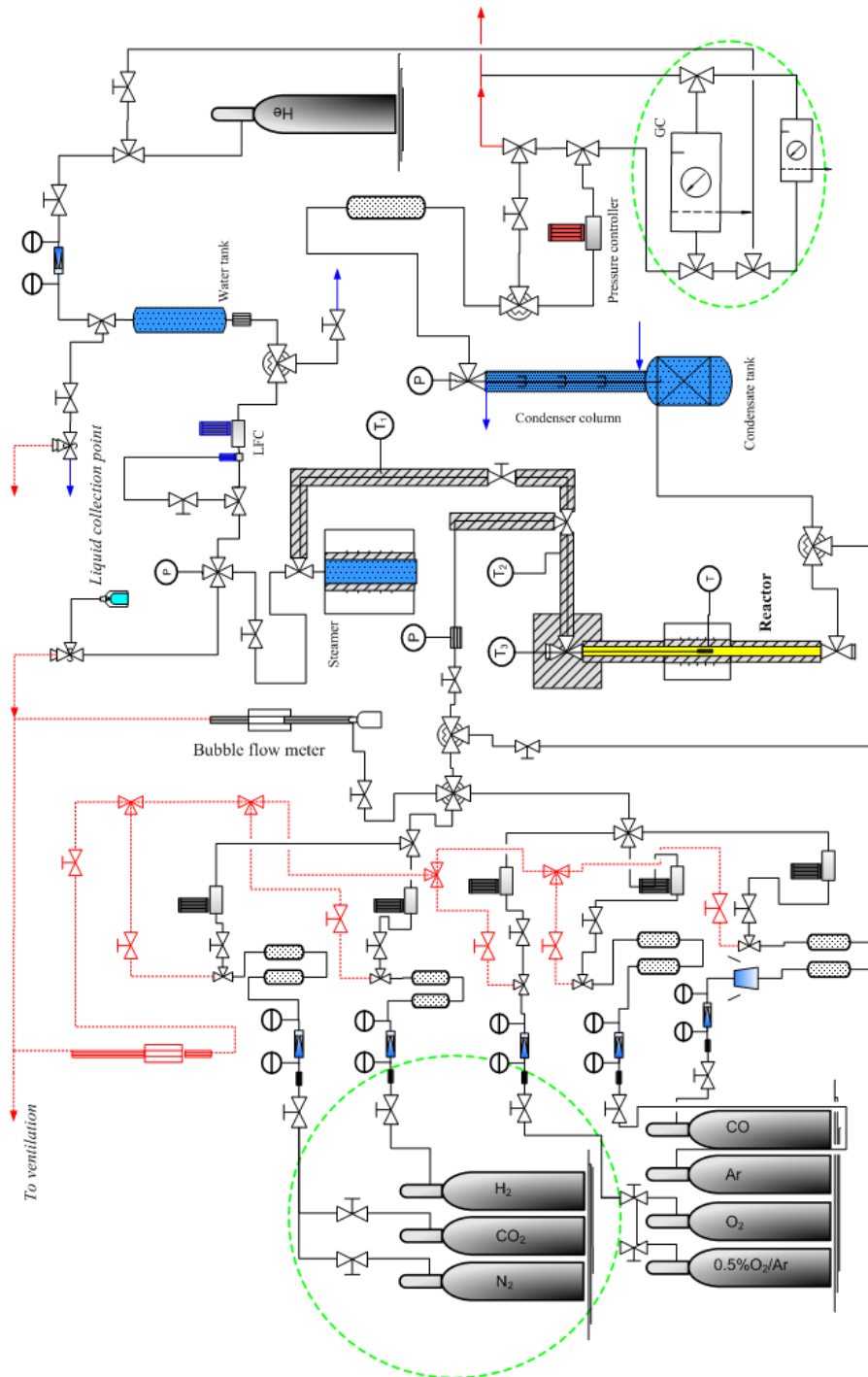
Figure A: Schematic diagram of setup [1]

Appendix B Risk assessment report

The report was built in 11.10.2016 in NTNU risk assessment system. All information can be found through website

https://avvik.ntnu.no/report?mk=risk

ID	13512		Status	Date
Risk Area	Risikovurdering: Helse, miljø og sikkerhet (HMS)		Created	11.10.2016
Created by	Jianyu Ma		Assessment started	11.10.2016
Responsible	Jianyu Ma		Actions decided	
			Closed	

CAT project/master 2017, Jianyu Ma

Valid from-to date:

10/11/2016 - 7/1/2017

Location:

3 - Gløshaugen / 316 - Kjemihallen / 1010 - 1. etasje / 100

Goal / purpose

This risk assessment contains the activities that involve the Metal dusting test setup located in the Chemistry Hall D 1st floor (Unit 1.1).

Background

The setup is connected to the ventilation
Furnace
Gas distribution system/cylinders

Description and limitations

Apparatus card attached

Prerequisites, assumptions and simplifications

All the users must get proper training before using the setup.

Attachments

apparatuscard 1.1.pdf

References

[Ingen registreringer]

Norges teknisk-naturvitenskapelige universitet (NTNU)	Print date:	Printed by:	Page:
Unntatt offentlighet jf. Offentlighetsloven § 14	06.06.2017	Jianyu Ma	1/12

63

Summary, result and final evaluation

The summary presents an overview of hazards and incidents, in addtition to risk result for each consequence area.

Hazard:	**Use of toxic/flammable gases**		

Incident:	**Fire, explosion**		

Consequence area:	Helse	Risk before actions: ●	Risiko after actions: ○
	Ytre miljø	Risk before actions: ●	Risiko after actions: ○
	Omdømme	Risk before actions: ●	Risiko after actions: ○

Incident:	**Inhalation/Leakage**		

Consequence area:	Helse	Risk before actions: ●	Risiko after actions: ○
	Ytre miljø	Risk before actions: ●	Risiko after actions: ○
	Omdømme	Risk before actions: ●	Risiko after actions: ○

Hazard:	**Use of flammable and toxic gases**		

Incident:	**Leakage**		

Consequence area:	Helse	Risk before actions: ●	Risiko after actions: ○
	Ytre miljø	Risk before actions: ●	Risiko after actions: ○
	Omdømme	Risk before actions: ●	Risiko after actions: ○

Hazard:	**Hot surfaces**		

Incident:	**skin burns**		

Consequence area:	Helse	Risk before actions: ●	Risiko after actions: ○
	Ytre miljø	Risk before actions: ●	Risiko after actions: ○
	Omdømme	Risk before actions: ●	Risiko after actions: ○

Hazard:	**Use of ethanol for cleaning**		

Incident:	**Spills on skin**		

Consequence area:	Helse	Risk before actions: ●	Risiko after actions: ○
	Ytre miljø	Risk before actions: ●	Risiko after actions: ○
	Omdømme	Risk before actions: ●	Risiko after actions: ○

Norges teknisk-naturvitenskapelige universitet (NTNU)	**Print date:**	**Printed by:**	**Page:**
Unntatt offentlighet jf. Offentlighetsloven § 14	06.06.2017	Jianyu Ma	2/12

64

Hazard:	Use of compressed gases (N2, He, Ar)				
Incident:	**Uncontrolled expansion and depleiton of O2**				
Consequence area:	Helse	Risk before actions:	●	Risiko after actions:	○
	Ytre miljø	Risk before actions:	●	Risiko after actions:	○
	Omdømme	Risk before actions:	●	Risiko after actions:	○

Incident:	**Gas leakage**				
Consequence area:	Helse	Risk before actions:	●	Risiko after actions:	○
	Ytre miljø	Risk before actions:	●	Risiko after actions:	○
	Omdømme	Risk before actions:	●	Risiko after actions:	○

Final evaluation

This risk assessment is performed for general use of the instrument. A copy of this risk assessment is placed next to the instrument.

All the users must be trained in order to use the instrument and they must read this Risk Assessment as well as the other information regarding HSE.

Norges teknisk-naturvitenskapelige universitet (NTNU)	**Print date:**	**Printed by:**		**Page:**
Unntatt offentlighet jf. Offentlighetsloven § 14	06.06.2017	Jianyu Ma		3/12

65

Units this risk assessment spans

- Institutt for kjemisk prosessteknologi

Participants

Xiaoyang Guo
Hilde Johnsen Venvik
Karin Wiggen Dragsten
Gunn Torill Wikdahl

Readers

[Ingen registreringer]

Others involved/stakeholders

[Ingen registreringer]

The following accept criteria have been decided for the risk area Risikovurdering: Helse, miljø og sikkerhet (HMS):

Helse	Materielle verdier	Omdømme	Ytre miljø

Norges teknisk-naturvitenskapelige universitet (NTNU)	**Print date:**	**Printed by:**	**Page:**
Unntatt offentlighet jf. Offentlighetsloven § 14	06.06.2017	Jianyu Ma	4/12

66

Overview of existing relevant measures which have been taken into account for this risk assessment

The table below presents existing measures which have been take into account when assessing the likelihood and consequence of relevant incidents.

Hazard	Incident	Mesaures taken into account
Use of toxic/flammable gases	Fire, explosion	HSE documentation
	Fire, explosion	Working alone regulations at NTNU
	Fire, explosion	Personal protective equipment
	Inhalation/Leakage	HSE documentation
	Inhalation/Leakage	Working alone regulations at NTNU
	Inhalation/Leakage	Personal protective equipment
Use of flammable and toxic gases	Leakage	HSE documentation
	Leakage	Working alone regulations at NTNU
	Leakage	Personal protective equipment
Hot surfaces	skin burns	HSE documentation
	skin burns	Working alone regulations at NTNU
	skin burns	Personal protective equipment
Use of ethanol for cleaning	Spills on skin	HSE documentation
	Spills on skin	Working alone regulations at NTNU
Use of compressed gases (N2, He, Ar)	Uncontrolled expansion and depleiton of O2	HSE documentation
	Uncontrolled expansion and depleiton of O2	Working alone regulations at NTNU
	Uncontrolled expansion and depleiton of O2	Personal protective equipment
	Gas leakage	HSE documentation
	Gas leakage	Working alone regulations at NTNU
	Gas leakage	Personal protective equipment
	Gas leakage	Installation and change of gas cylinders
	Gas leakage	gas-detectors
	Gas leakage	All users get proper training before using this unit

Existing relevant measures with descriptions:

HSE documentation
The laboratories have an updated Room Card and the unit 1.1 has a copy of the risk assessment, operating instructions and apparatus card with information regarding safety and information in case of emergency stop.

Different phone numbers are provided to contact in case of emergency.

Working alone regulations at NTNU
NTNU students and employee are not allowed to work alone after 7pm and during the weekends.

Working after 19:00 or in the weekends, you need to be at least 2 in the lab or in the building with regularly check-ups (every 30 minutes). Both of the people needs to have access to the labs

Norges teknisk-naturvitenskapelige universitet (NTNU)	Print date:	Printed by:		Page:
Unntatt offentlighet jf. Offentlighetsloven § 14	06.06.2017	Jianyu Ma		5/12

67

Personal protective equipment

The hall contains googles, other safety measures and a first-aid kit.. There are also gloves, lab coats and more protective equipment available upon request.

Ventilation

The unit is connected to the ventilation system. The door must be closed when the unit is in use.

Leak test

Should use googles, gloves and lab coat when operating the set-up.

Installation and change of gas cylinders

Only performed by authorized personnel.

gas-detectors

The set-up is placed inside a plastic box with ventilation and CO, CH4 and H2 gas-detectors

All users get proper training before using this unit

[Ingen registreringer]

Risk analysis with evaluation of likelyhood and consequence

This part of the report presents detailed documentation of hazards, incidents and causes which have been evaluated. A summary of hazards and associated incidents is listed at the beginning.

The following hazards and incidents has been evaluated in this risk assessment:

- **Use of toxic/flammable gases**
    - Fire, explosion
    - Inhalation/Leakage
- **Use of flammable and toxic gases**
    - Leakage
- **Hot surfaces**
    - skin burns
- **Use of ethanol for cleaning**
    - Spills on skin
- **Use of compressed gases (N2, He, Ar)**
    - Uncontrolled expansion and depleiton of O2
    - Gas leakage

Overview of risk mitigating actions which have been decided, with description:

Norges teknisk-naturvitenskapelige universitet (NTNU)	Print date:	Printed by:		Page:
Unntatt offentlighet jf. Offentlighetsloven § 14	06.06.2017	Jianyu Ma		6/12

68

Use of toxic/flammable gases (hazard)

Use of toxic/flammable gases/Fire, explosion (incident)

Overall assessed likelihood of the incident: Unlikely (1)

Comment to likelihood assessment:

[Ingen registreringer]

Assessment of risk for the consequence area: Helse

Assessed likelihood (common for incident):   Unlikely (1)

Assessed consequence: Medium (2)

Comment to consequence assessment:

[Ingen registreringer]

Use of toxic/flammable gases/Inhalation/Leakage (incident)

Overall assessed likelihood of the incident: Unlikely (1)

Comment to likelihood assessment:

[Ingen registreringer]

Assessment of risk for the consequence area: Helse

Assessed likelihood (common for incident):   Unlikely (1)

Assessed consequence: Medium (2)

Comment to consequence assessment:

[Ingen registreringer]

Norges teknisk-naturvitenskapelige universitet (NTNU)	**Print date:**	**Printed by:**	**Page:**
Unntatt offentlighet jf. Offentlighetsloven § 14	06.06.2017	Jianyu Ma	7/12

69

Use of flammable and toxic gases (hazard)

Use of flammable and toxic gases/Leakage (incident)

Overall assessed likelihood of the incident: Less likely (2)

Comment to likelihood assessment:

[Ingen registreringer]

Assessment of risk for the consequence area: Helse

Assessed likelihood (common for incident):   Less likely (2)

Assessed consequence: Medium (2)

Comment to consequence assessment:

[Ingen registreringer]

Hot surfaces (hazard)

Hot surfaces/skin burns (incident)

Overall assessed likelihood of the incident: Less likely (2)

Comment to likelihood assessment:

[Ingen registreringer]

Assessment of risk for the consequence area: Helse

Assessed likelihood (common for incident):   Less likely (2)

Assessed consequence: Medium (2)

Comment to consequence assessment:

[Ingen registreringer]

**Norges teknisk-naturvitenskapelige
universitet (NTNU)**

Unntatt offentlighet jf. Offentlighetsloven § 14

Print date:

06.06.2017

Printed by:

Jianyu Ma

Page:

8/12

70

Use of ethanol for cleaning (hazard)

Use of ethanol for cleaning/Spills on skin (incident)

Overall assessed likelihood of the incident: Less likely (2)

Comment to likelihood assessment:

[Ingen registreringer]

Assessment of risk for the consequence area: Helse

Assessed likelihood (common for incident): Less likely (2)

Assessed consequence: Small (1)

Comment to consequence assessment:

[Ingen registreringer]

Use of compressed gases (N2, He, Ar) (hazard)

Use of compressed gases (N2, He, Ar)/Uncontrolled expansion and depleiton of O2 (incident)

Overall assessed likelihood of the incident: Unlikely (1)

Comment to likelihood assessment:

[Ingen registreringer]

Assessment of risk for the consequence area: Helse

Assessed likelihood (common for incident): Unlikely (1)

Assessed consequence: Medium (2)

Comment to consequence assessment:

[Ingen registreringer]

Norges teknisk-naturvitenskapelige universitet (NTNU)	**Print date:**	**Printed by:**	**Page:**
Unntatt offentlighet jf. Offentlighetsloven § 14	06.06.2017	Jianyu Ma	9/12

71

Use of compressed gases (N2, He, Ar)/Gas leakage (incident)

Overall assessed likelihood of the incident: Unlikely (1)

Comment to likelihood assessment:

[Ingen registreringer]

Assessment of risk for the consequence area: Helse

Assessed likelihood (common for incident): Unlikely (1)

Assessed consequence: Small (1)

Comment to consequence assessment:

[Ingen registreringer]

Norges teknisk-naturvitenskapelige universitet (NTNU) **Print date:** **Printed by:** **Page:**

Unntatt offentlighet jf. Offentlighetsloven § 14 06.06.2017 Jianyu Ma 10/12

72